Journal of Structural Geology 140 (2020) 104163

Contents lists available at ScienceDirect

Journal of Structural Geology

journal homepage: http://www.elsevier.com/locate/jsg

The role of structural inheritance in the development of high-displacement crustal faults in the necking domain of rifted margins: The Klakk Fault Complex, Frøya High, offshore mid-Norway

Jhon M. Muñoz-Barrera [*], Atle Rotevatn, Rob L. Gawthorpe, Gijs A. Henstra [1], Thomas B. Kristensen [2]

University of Bergen, Realfagbygget, Allégaten 41, 5007, Bergen, Norway

ARTICLE INFO

Keywords:
Multiphase rifting
High-displacement low-angle normal fault
3D fault geometry
Intra-basement structures
Supradetachment basin
Metamorphic core complex

ABSTRACT

The role of inherited structures during the development of normal faults in continental rifts and proximal domains of passive margins have been extensively studied. Few studies, however, have a focus on deciphering the role of inheritance in the development of high-displacement (>10 km), low-angle (<30°) normal faults in necking domains of passive margins. We integrated and interpreted potential field, 2D and 3D reflection seismic, and well data to study the role of structural inheritance in controlling the location and development of the southern part of the Klakk Fault Complex, offshore mid-Norway. The down-to-the-west Klakk Fault Complex is an N-S non-collinear fault complex that separates the Frøya High in its footwall from the Rås Basin in its hanging wall. The fault segments vary from low-angle planar to listric fault geometries in cross-section, with displacements of 17 km–34 km. These displacements led to syn-rift basement thinning of 12–14 km toward the west, which consequently, also affected the crustal wedge geometry of the necking domains. We identify three intra-acoustic-basement structures based on seismic facies and define their 3D geometry: (i) a bowl-shaped basin, (ii) a hyperbolic surface, and (iii) a domal structure. We discuss their origin and elucidate their role during later rifting. We conclude that pre-existing basement structures controlled the rift-related structures during the second rift phase (thinning), and affected the location, geometries, orientation and segmentation of the high-displacement low-angle faults in the necking domains. The results of this work offer new insights into the development of necking domains in areas where a thick continental crust (>25 km) is present during rifting.

1. Introduction

The magma budget, development and final geometry of continental rifts and rifted margins are controlled by the interplay between structural inheritance and extensional tectonics, along with such factors as the strength, thickness, composition, and thermal structure of the crustal lithosphere (Doré et al., 1997; Chenin et al., 2015; Manatschal et al., 2015; Rotevatn et al., 2018; Salazar-Mora et al., 2018; Schiffer et al., 2019). Several studies have demonstrated that pre-existing structures may (i) be subject to reactivation during extension/shortening (Daly et al., 1989; Theuniseen et al., 1996; Fossen, 2010; Phillips et al., 2016; Fazlikhani et al., 2017), (ii) control the nucleation and localisation of new faults during rifting (Manatschal et al., 2015; Deng et al., 2017; Collagena et al., 2019), (iii) cause stress field perturbation and formation of non-collinear fault networks (Morley et al., 2004; Reeve et al., 2015; Deng et al., 2017; Collagena et al., 2019; Osagiede et al., 2020), (iv) control the segmentation of faults and rift basins (Katumwehe et al., 2015; Rotevatn et al., 2018), (v) influence the length, orientation, spacing and evolution of faults (Fossen and Rotevatn, 2016; Deng et al., 2017; Osagiede et al., 2020), and vi) control the shape and evolution of the necking zones (Manatschal et al., 2015). Improvements in seismic quality and computer capacity during the last two decades have improved imaging of the intra-basement structures in seismic reflection data, the 2D & 3D modelling, and allow identification of how some of

* Corresponding author.
E-mail addresses: jhon.munoz@uib.no (J.M. Muñoz-Barrera), atle.rotevatn@uib.no (A. Rotevatn), rob.gawthorpe@uib.no (R.L. Gawthorpe), gijshenstra@gmail.com (G.A. Henstra), thomas.berg.kristensen@gmail.com (T.B. Kristensen).
[1] Current address: Aker BP, Oksenøyveien 10, 1366 Lysaker, Norway.
[2] Current address: Equinor, Sandsliveien 90, 5254 Sandsli, Norway.

https://doi.org/10.1016/j.jsg.2020.104163
Received 7 February 2020; Received in revised form 5 August 2020; Accepted 8 August 2020
Available online 17 August 2020

these structures control the location, orientation and interaction of rift-related faults (Bird et al., 2015; Manatschal et al., 2015; Phillips et al., 2016; Deng et al., 2017; Fazlikhani et al., 2017; Lenhart et al., 2019; Wrona et al., 2019). Some of these seismic studies show that thicker shear zones with a dip >15° tend to be reactivated (Phillips et al., 2016; Fazlikhani et al., 2017). Thick shear zones are up to 300 km thick, up to 50 km long with displacements up to 10 km (See by Wrona et al., 2019 for a compilation of outcropped shear zones). Outcrop and seismic studies have shown the geometries of the shear zones in map view and cross-section, but their three-dimension geometry is still unknown. In addition, despite the number of studies devoted to deciphering the interaction between inheritance structures and rift-related faults, these studies have focused primarily on continental rifts and the proximal domains of rifted margins. It is, therefore, largely unknown how inherited structures impact later stages of rifting and passive margin development, including the role of pre-existing fabric in controlling the development of high-displacement (>3 km), low-angle (<30°) normal faults.

Long-lived faults with moderate to low-angle dip and tens of kilometres displacement delimit the different structural domains along-and-across strike of rifted margins (Fig. 1) (Osmundsen and Péron-Pinvidic, 2018; Ribes et al., 2019). Highly extended terranes, such as metamorphic core complexes or hyperextended margins, have given insight into the behaviour of these faults (Davis, 1980; Lister et al., 1986; Andersen and Jamtveir, 1990; Malavieille, 1993; Davis et al., 2002; Axen, 2004; Manatschal, 2004; Sutra and Manatschal, 2012; Peron-Pinvidic et al., 2013). Based on some of these studies and seismic examples of the Norwegian passive margin, Osmundsen and Péron-Pinvidic (2018) name the low-angle, highly-displacement faults as High-β faults, and classified them in three types regarding deformation processes and the thickness of the continental crust (Fig. 1). (i) High-β 'type 0' faults (type HB0 late-to post-orogenic detachment) are detachment faults associated with the evolution of metamorphic core complexes and supradetachment basins generated during late-to post--contractional stages of the Caledonian orogenic events, which are now preserved in the proximal domains of the margin (Braathen et al., 2000; Fossen, 2010; Gee et al., 2010; Corfu et al., 2014). These faults display listric, subhorizontal or convex geometries in cross-section with displacements of up to 100 km. (ii) High-β 'type 1' faults (type HB1: coupling detachment) are faults related to the crustal thinning in the necking domain of rifted margins. These faults have planar, listric or ramp-flat geometries, dips of 0–45° and displacements of 20 km–30 km in cross-section. Geometry variation along strike depends on the thickness, thermal state, composition and presence of ductile layers within the continental crust, and hence the efficiency of the coupling process between the continental crust and mantle (Manatschal et al., 2015; Osmundsen and Péron-Pinvidic, 2018). (iii) High-β 'type 2' faults (type HB2: exhumation detachment) are low angle (<30°) faults with listric, horizontal to convex-upwards geometries in cross-section. These faults are located in the distal domains of hyperextended rifted margins and have displacement up to 100 km.

This paper builds on the work of Osmundsen and Péron-Pinvidic (2018), investigating how inherited basement structures controlled the location, geometry, orientation and segmentation of High-β 'type 1' fault complexes developed during later rift phases within a thick continental crust (>25 km). To do this, we focus on the southern part of the Klakk Fault Complex (Klakk FC), which is located in the southern transition between the Møre and Vøring margin segments of the Norwegian Passive Margin (Mosar, 2003) (Fig. 2a). The Klakk FC separated the Frøya High-Sklinna Ridge in its footwall from the Rås Basin in its hanging wall during the late Jurassic and early Cretaceous rifting episodes (Fig. 2b). The Klakk FC is associated with a thinning of the continental crust from

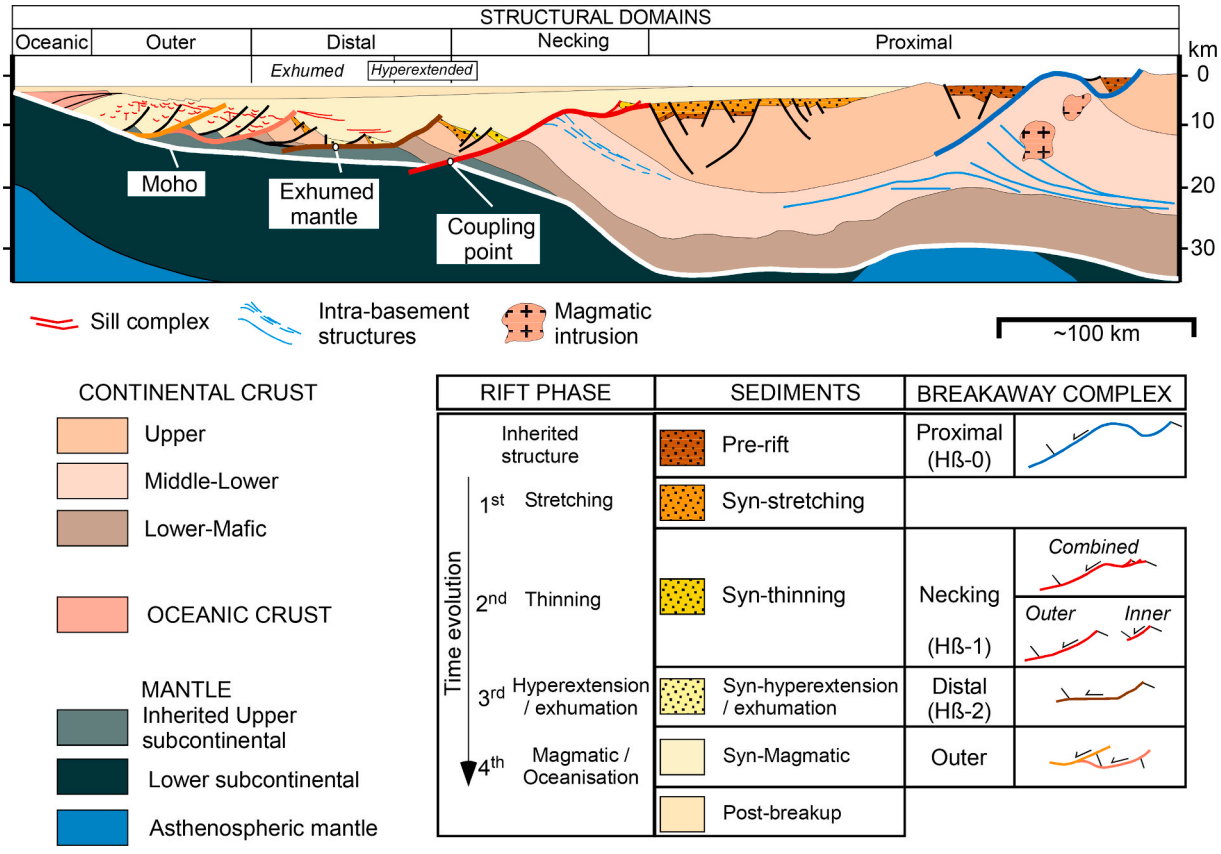

Fig. 1. Schematic section of a typical rifted margin adapted on illustrations by Masini et al. (2012), Péron-Pinvidic et al. (2013) and Osmundsen and Péron-Pinvidic (2018). Breakaway complexes based on Osmundsen and Péron-Pinvidic (2018). Rift phases based on Naliboff et al. (2017).

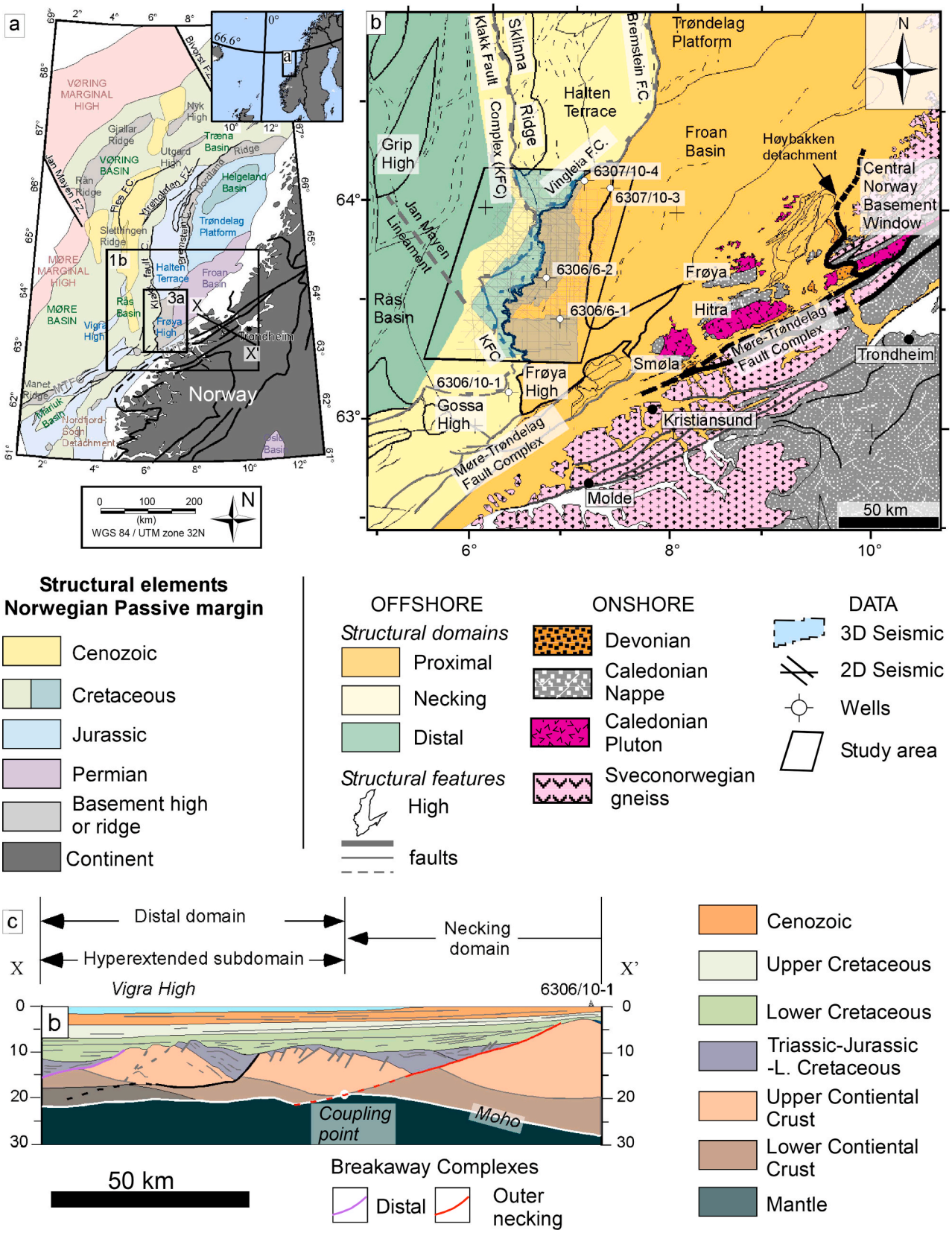

Structural elements Norwegian Passive margin

- Cenozoic
- Cretaceous
- Jurassic
- Permian
- Basement high or ridge
- Continent

OFFSHORE

Structural domains
- Proximal
- Necking
- Distal

Structural features
- High
- faults

ONSHORE
- Devonian
- Caledonian Nappe
- Caledonian Pluton
- Sveconorwegian gneiss

DATA
- 3D Seismic
- 2D Seismic
- Wells
- Study area

Fig. 2. Location of the study area. (a) Map of the mid-Norwegian rifted margin showing the main structural elements (after Osmundsen et al., 2016), the general location of the study area and location of cross-section X-X'. (b) General structural map of the study area and location of wells and seismic data used in this work. Onshore geological map compiled from Mosar (2003), Braathen et al. (2000) and Blystad et al. (1995). Offshore structural domains based on Peron-Pinvidic et al. (2013). Offshore fault configuration adapted from Blystad et al. (1995). (c) cross-section X-X' adapted from Osmundsen et al. (2016).

c. 30 km to *c.* 10 km, and thus, a crustal wedge geometry (Fig. 2c) (Osmundsen et al., 2002; Osmundsen and Redfield, 2011; Peron-Pinvidic et al., 2013; Osmundsen and Péron-Pinvidic, 2018). We constructed a 3D structural model of Klakk FC and surrounding area, integrating and interpreting 3D and 2D seismic reflection, well and potential field data to the west of the Frøya High (Fig. 2b). We show that the Klakk FC comprises N-S striking non-collinear fault complex, which has planar, listric and convex geometries in cross-section, with displacements of 17 km–34 km. We map several discrete basement structures and elucidate the controls they exerted on the geometry and evolution of the Klakk FC. The high quality seismic, with good imaging of structures to 10 s TWT depth, combined with the potential field data available, make this area a locality type for the study of High-β 'type 1' faults within a thick continental crust.

2. Structural style of rifted margins

The structural configuration of a typical rifted margin is composed of proximal, necking, distal, outer and oceanic domains (Fig. 1) (Peron-Pinvidic et al., 2013). Proximal domains are characterised by low values of extension where a continental crust exceeds 30 km thickness. Faults show steeply-dipping planar to listric geometries (low-β faults) that define half-grabens (Gawthorpe et al., 2000; Manatschal, 2004; Peron-Pinvidic et al., 2013; Osmundsen and Péron-Pinvidic, 2018). Necking domains display a continental crust wedge shape (>10 km to < 30 km) in cross-section, which is produced by rapid strain localisation onto High-β 'type 1' faults (Osmundsen and Ebbing, 2008; Peron-Pinvidic et al., 2013; Naliboff et al., 2017). High-β 'type 1' faults developed in a thick continental crust with a steep geothermal gradient may generate CMCC in the necking domains (Osmundsen and Péron-Pinvidic, 2018). The distal domain is an area where extension affects a continental crust that is less than 10 km thick. It is divided into two subdomains, hyperextended and exhumed (Fig. 1) (Peron-Pinvidic et al., 2013). Sag-basin types characterise this domain, where the footwall size decreases oceanward (Fig. 1) (Manatschal, 2004; Sutra et al., 2013). The High-β faults that limit the different structural domains have been denominated as breakaway complexes (Fig. 1). (i) proximal breakaway complex limits the non-rifted area from the proximal domain; (ii) inner necking breakaway complex separates the proximal domain from the necking domain; (iii) outer necking breakaway complex delimits the necking domain from the distal domain; (iv) distal breakaway complex limits the hyperextended subdomain from the exhumed subdomain; and (v) outer breakaway complex bounds the exhumed subdomain from the outer domain. In this paper, and following Osmundsen and Péron-Pinvidic (2018), the terms inner necking, outer necking, and combined inner and outer necking breakaway complexes are used to describe the High-β 'type 1' faults that interact in the necking domain.

3. Intra-basement structures

Inherited structures in continental rifts and rifted margins are generally defined as pre-rift basement structures such as continental metamorphic core complexes, continental supradetachment basins, shear zones, ancient thrust or normal faults, and pervasive basement fabrics (e.g. Reeve et al., 2014; Phillips et al., 2016; Fazlikhani et al., 2017; Lenhart et al., 2019). High-displacement normal faults may exhume rocks from the middle and lower continental crust generating continental metamorphic core complexes in areas where the continental crust is more than 30 km thick (Davis, 1980; Wernicke, 1981; Serenne and Seguret, 1987). These metamorphic core complexes tend to display elongate domal geometries with major axis parallel or perpendicular to the extension direction, or hyperbolic geometries with marked asymmetries parallel and perpendicular to the extension direction (Jolivet et al., 2010; Wiest et al., 2019). Metamorphic core complexes have been divided into continental core complexes (CCC), continental margin core complexes (CMCC) and oceanic core complexes based on the thickness or absence of continental crust (Whitney et al., 2013). Supradetachment basins form above high-displacement normal faults, and they record the evolution of the highly extended terranes (Friedmann and Burbank, 1995; Osmundsen et al., 1998; Vetti and Fossen, 2012).

Shear zones form tabular zones from cms to several kms thickness and up to 100 s km in length, which can accommodate large amounts of strain during extension, shortening and/or strike-slip movement (Fossen and Cavalcante, 2017; Wrona et al., 2019). Detachment zones are shear zones that flatten into the brittle-ductile transition zone. Shear zones in seismic images can be identified based on three geometries: multiple inclined reflections, converging reflections and cross-cutting reflections (Wrona et al., 2019). Such geometries may, however, also represent layered basement, metamorphosed sedimentary rocks, or magmatic intrusions, which adds uncertainty to the seismic interpretation (Phillips et al., 2016; Fazlikhani et al., 2017; Wrona et al., 2019). Despite shear zones having been recognised in outcrop and seismic images (Fossen, 2010; Phillips et al., 2016; Wiest et al., 2019; Osagiede et al., 2020), their 3D geometry has not been well identified, because it may display a combination of highs and lows, in both sense, parallel or perpendicular to the movement direction (Lenhart et al., 2019; Wiest et al., 2019). Improvements in the acquisition and computational power have been increasing the quality of the recent reflection seismic surveys. They may illuminate metamorphic core complexes, supradetachment basins, shear zones and pre-existing faulting as part of the intra-basement structures (Reeve et al., 2014; Bird et al., 2015; Phillips et al., 2016; Fazlikhani et al., 2017; Collagena et al., 2019; Lenhart et al., 2019; Trice et al., 2019; Osagiede et al., 2020).

4. Geological background

The Norwegian passive margin has a NE-SW to N-S trend, with three dominant NW-SE-trending fracture zones (Jan Mayen, Bivrost and Senja) that divide the rifted margin into three main segments: Møre, Vøring and Lofoten-Vesterålen (Fig. 2a) (Blystad et al., 1995; Mosar, 2003; Faleide et al., 2008, 2010; Peron-Pinvidic et al., 2013; Osmundsen et al., 2016; Osmundsen and Péron-Pinvidic, 2018).

4.1. Regional tectonics

The closure of the Iapetus Ocean during the Ordovician and the subsequent oblique continent-continent collision between Laurentia and Baltica during the Silurian resulted in the culmination of the Caledonian orogeny (Torsvik and Cocks, 2005; Gee et al., 2013). This mountain belt featured major thrust and nappe units with an overall eastward to southeastward vergence that involved rocks from Baltica, Laurentia, Iapetus Ocean and exotic, predominantly island arc terrains (Gee et al., 2010, 2013; Corfu et al., 2014). The onshore geology in Western Norway offers insight into the Caledonian basement structure and composition, which acted as a 'structural template' for later rifting (Fossen, 2010; Chenin et al., 2015; Lenhart et al., 2019; Schiffer et al., 2019).

Post-orogenic collapse, from 403 to 380 Ma (Fossen, 2000, 2010), generated a series of continental core complex-style basement culminations along the Norwegian margin, including the Western Gneiss Region (WGR) and the Central Norwegian Basement Window (CNBW) (Fig. 2a and b and) (Braathen et al., 2000; Osmundsen and Andersen, 2001; Osmundsen et al., 2006; Fossen, 2010; Andersen et al., 2012; Corfu et al., 2014; Fossen et al., 2016). Orogenic collapse also led to the formation of a series of extensional detachments that bounded intra-montane Devonian collapse basins (Braathen et al., 2000; Osmundsen and Andersen, 2001; Osmundsen et al., 2006). Examples of these extensional detachment shear zones include the Nordfjord-Sogn Detachment Zone, which bound the Solund, Kvamshesten, Håsteinen and Hornelen basins in the WGR, and the Høybakken Detachment, which bounds the 'Old Red Sandstone' basins in the CNBW (Fig. 2b) (Braathen et al., 2000, 2002; Osmundsen and Andersen, 2001; Eide

et al., 2005; Skilbrei and Olesen, 2005; Osmundsen et al., 2006; Corfu et al., 2014; Fossen et al., 2016; Lenhart et al., 2019).

Péron-Pinvidic and Osmundsen (2018) suggest that the prolonged, multi-phase rifting history of the mid-Norwegian margin was the result of the interaction between four deformation phases: stretching, thinning, exhumation-hyperextension and oceanisation-break up. The first rifting phase (stretching) includes mild rifting episodes during the mid-Carboniferous and a more significant rifting episode during the Permian- Lower Triassic (Blystad et al., 1995; Doré et al., 1999; Faleide et al., 2010; Tsikalas et al., 2012). Widespread extension created half-grabens with preferential NNE and NE strike during this episode, now preserved in the proximal domain (e.g. Froan Basin and Trøndelag Platform) (Fig. 2b) (Blystad et al., 1995; Doré et al., 1999; Müller et al., 2005; Peron-Pinvidic et al., 2013). The second rifting phase (thinning) consists of mild rifting events during the early Jurassic focused on the Halten Terrace, and a major rifting episode during the latest Middle Jurassic to Late Jurassic, which localised on the boundary between the Trøndelag Platform and the Rås and Træna basins. This rift phase caused high-β faults to form (e.g. Klakk FC, Bremstein Fault Complex, Ytreholmen Fault Complex and Vingleia Fault Complex) and, consequently, the wedge-shaped crustal geometry of the necking domain in cross-section (Figs. 1 and 2) (Doré et al., 1999; Osmundsen and Ebbing, 2008; Elliott et al., 2012; Peron-Pinvidic et al., 2013; Bell et al., 2014; Ravnås et al., 2014). The third rifting phase (exhumation-hyperextension) was a major rifting event during the earliest Cretaceous and a middle Cretaceous mild rifting (Blystad et al., 1995; Doré et al., 1997, 1999; Faleide et al., 2010; Péron-Pinvidic and Osmundsen, 2018). Extension during this phase was focused mainly on the Rås Basin and created hyperextended and sag basins, with associated mantle exhumation and serpentinisation (Peron-Pinvidic et al., 2013; Osmundsen et al., 2016; Péron-Pinvidic and Osmundsen, 2018). The fourth rifting phase (oceanisation-break up) involved major rifting during the Late Cretaceous-earliest Eocene (Blystad et al., 1995; Doré et al., 1999; Faleide et al., 2010; Gernigon et al., 2012; Péron-Pinvidic and Osmundsen, 2018). Extension in this phase localised mainly in the distal domain, producing the Møre and Vøring marginal highs, and ultimately leading to a continental breakup between *c.* 52 to 49 Ma (Gernigon et al., 2012). The margins currently display an NW tilting because of thermal subsidence since the middle Cretaceous (Bell et al., 2014).

4.2. Study area

4.2.1. Structures

This paper focuses on the area around the boundary between the Møre and the Vøring Basins, one of the boundaries between two of the Norwegian margin mega-segments. We focus on the area around the Frøya High, specifically the Klakk FC. This fault complex separates the Frøya High in its footwall from the Rås Basin in its hanging wall, which was active during the late Jurassic and early Cretaceous rifting episodes (Figs. 2 and 3) (Blystad et al., 1995; Faleide et al., 2010; Osmundsen et al., 2016). The Klakk FC has an overall N-S strike and is *c.* 270 km long. The Klakk FC has a westward dip and features heaves of 10–15 km (Blystad et al., 1995; Osmundsen et al., 2016; Osmundsen and Péron-Pinvidic, 2018). Osmundsen and Péron-Pinvidic (2018) suggest that the Klakk FC represents a combined inner and outer necking breakaway complex along the Frøya High, whereas this fault complex represents the outer necking breakaway zone in the Sklinna Ridge area (Fig. 2b).

The Klakk FC interacts southwards with the Jan Mayen Lineament (JML) and the Møre-Trøndelag Fault Complex (MTFC) (Fig. 2a and b and). The JML represents the southwestward continuation of the sinistral NW-SE trending Jan Mayen transform fault system, and it separates the Møre Basin from the Vøring Basin, Halten Terrace and Frøya High (Fig. 2a and b and) (Blystad et al., 1995). The MTFC separates the northern Viking Graben from the Møre Margin (Gabrielsen et al., 1999; Nasuti et al., 2012). The down-to-the-NW MTFC strikes ENE to NE, is *c.* 750 long, and is composed of several fault segments in a zone up to *c.* 80 km wide. Osmundsen and Péron-Pinvidic (2018) define the southeastern strand of the MTFC in the Møre margin segment as the proximal breakaway complex, whereas the northwestern strand comprises the outer necking breakaway complex (Fig. 2b and c and). This fault complex underwent dextral movement during the Silurian (Seranne, 1992; Doré et al., 1997), sinistral movement during the Devonian (Seranne, 1992; Braathen et al., 2000; Osmundsen et al., 2006), and several brittle dip-slip to oblique-slip and dextral displacement events since the late Palaeozoic (Braathen et al., 2002; Redfield et al., 2005).

The Klakk FC interacts northwards with the Vingleia Fault Complex (VFC). The NE-trending VFC separates the Frøya High from the Halten Terrace to the north (Fig. 2b). The VFC was active during the Triassic, with major displacement accommodation during the main late Jurassic and early Cretaceous rifting phases (Ravnås et al., 2014; Elliott et al., 2015; Osmundsen et al., 2016). The Vingleia Fault Complex joins the N-S trending Bremstein Fault Complex towards the northeast, where it is the inner necking breakaway complex of the Vøring margin segment (Fig. 2a and b and) (Osmundsen et al., 2016; Osmundsen and Péron-Pinvidic, 2018).

4.2.2. Basement lithologies

The Central Norway Basement Window (CNBW) and the Frøya High are part of the same crystalline basement, based on the similarity in both their exhumation ages and geophysical characteristics (Skilbrei et al., 2002; Eide et al., 2005; Osmundsen et al., 2005). The CNBW, therefore, is an onshore analogue for the Frøya High. The CNBW is a continental core complex that was uplifted by the interplay of the MTFC with the Høybakken and the Kolstraumen detachments during the orogenic-collapse, *c.* 400-365 Ma (Braathen et al., 2000, 2002; Kendrick et al., 2004; Eide et al., 2005; Osmundsen et al., 2006). Proterozoic crystalline rocks overlain by a thin folded layer of rocks of the Seve Nappe (Middle Allochthon) represent the lower plate, whereas upper-, uppermost-allochthon rocks (Caledonian intrusions, supracrustal rocks) and Upper Devonian 'Old Red sandstone' basins composes the upper plate of the continental core complex (Fig. 2) (Eide et al., 2005; Gee et al., 2010; Corfu et al., 2014; Robinson et al., 2015). Four boreholes have drilled the basement on the Frøya High with granite crystalline basement being reported. Core into the basement (2972 m–2672.6 m) was recovered from borehole 6407/10-3. Slagstad et al. (2011) classify a sample from this core as a fine-cal-alkaline granite of syn-collisional volcanic arc affinity, with a crystallisation age of 437 ± 4 Ma using U-Pb in zircons. In addition, they propose that these rocks are part of the uppermost allochthones of the Caledonian nappe and correlate them with the granite rocks outcropped at Smøla and Hitra islands. Eide et al. (2005) determine an exhumation age of 377 ± 3.4 Ma for the same core using 40Ar/39Ar method, which is similar to the ages reported for the Høybakken detachment using the same dating method (Kendrick et al., 2004).

The Frøya High is covered by several geophysical surveys, including potential fields and seismic reflection data. The Frøya High is characterised by strong positive magnetic and gravity anomalies (>1200 nT and >60 mGal, respectively) (Fig. 3) (Skilbrei et al., 2002; Skilbrei and Olesen, 2005; Olesen et al., 2010, 2010b; Maystrenko et al., 2018). Gravity anomaly values in the Frøya High may reflect a high-density lower-crustal granulite layer (Mjelde et al., 2016; Maystrenko et al., 2018), or Precambrian rocks similar to the CNBW with intrusions of Caledonian plutons (Skilbrei and Olesen, 2005). The magnetic anomaly has been interpreted as a highly uplifted granitic to dioritic crystalline Precambrian rock based on a correlation with onshore rocks (Skilbrei et al., 2002; Skilbrei and Olesen, 2005; Maystrenko et al., 2018). Seismic data reveal an intra-basement antiformal structure underneath the Vingleia Fault Complex (VFC), which has been interpreted as a Palaeozoic shear zone (Osmundsen et al., 2002, 2005, 2016; Skilbrei and Olesen, 2005). Outcrops, boreholes, potential field and seismic data, therefore, suggest that both, the CBNW and the Frøya High are

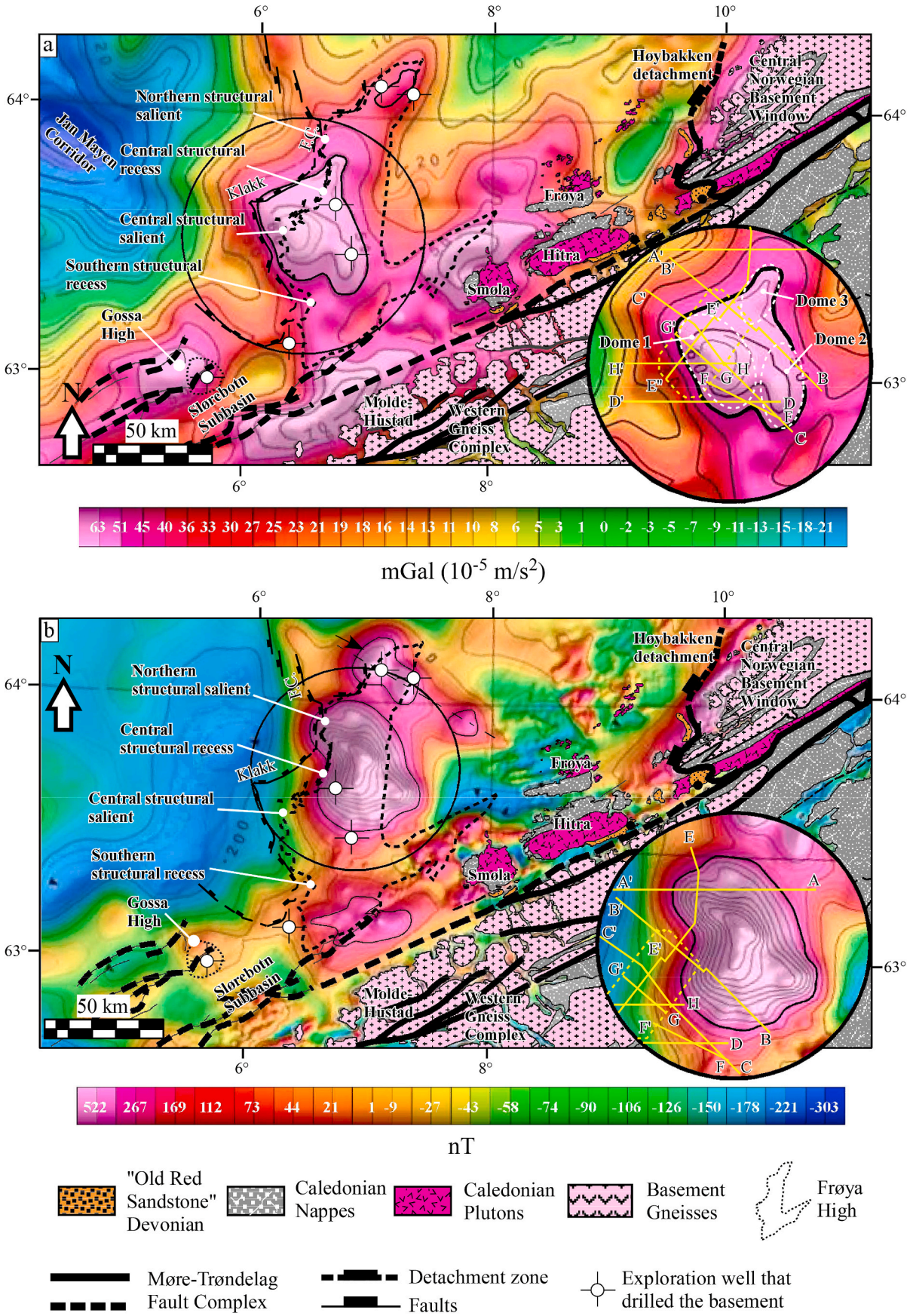

Fig. 3. Geological map compiled from Braathen et al. (2000), Blystad et al. (1995) Mosar (2003) & Skilbrei and Olesen (2005). (a) Gravity anomaly map (Olesen et al., 2010). Values displayed has isostasy-corrected free air anomalies and isostasy-corrected Bouguer anomaly values using rock density of 2.670 kg/m3. (b)

Magnetic anomaly map (Olesen et al., 2010b). Anomaly values extracted from total magnetic values using Definite Geomagnetic Reference Field (DGRF) on single grid.

continental core complexes generated by orogenic collapse during the Devonian (Osmundsen et al., 2005).

5. Data and methods

5.1. Data

We use information from four boreholes that penetrated the basement rocks of the Frøya High, six 3D seismic surveys (4438 km^2), a selection of 2D lines from eleven seismic surveys (11148 km total length), and the gravity anomaly and magnetic anomaly maps of Olesen et al., 2010 and Olesen et al. (2010b) (Figs. 2 and 3 and Tables 1 and 2). Seismic surveys recorded information to maximum depths of five and 10 s TWT. These data were processed in zero-phase and are displayed here in reverse polarity (Society of Exploration Geophysicists [SEG]). Black colour reflections (peak) in the seismic sections represents an increase in acoustic impedance, while red colour reflection (trough) denotes a decrease in acoustic impedance.

5.2. Methods

We integrated and interpreted the seismic data and well information in Petrel 2016 for software), and we used structural smoothing attribute to reduce the noise-signal ratio in the seismic data. This attribute improves the continuity of basement reflections. VSP data of each well was used to tie the geological data with the seismic data (Table 1). The top of the acoustic basement is characterised by a high-amplitude peak reflection (e.g. Fig. 5a and b and). Fault geometries were defined using the methodology by Shaw et al. (2004), which is based on (i) direct fault-plane reflections, produced by changes in acoustic impedance across and within fault zones, (ii) terminations of fold limbs or kink bands, and (iii) fault cutoffs (terminations of reflections or abrupt changes of reflection attributes at the fault surface). Fault planes were mapped using the fault interpretation strategies described by Tearpock and Bischke (2003). We classified intra-basement reflectivity into different seismic facies based on amplitude, geometry and continuity characteristics. The contacts and overall geometry of these seismic facies were identified and mapped to define the geometry of intra-basement structures. Comparison between different overlapping 2D and 3D surveys allowed recognition of geophysical artefacts (Fazlikhani et al., 2017). The layer cake methodology by Marsden (1989) was used for depth conversion using Move software. We calculated average velocities from VSP reports from the Cenozoic and Upper Cretaceous succession. The velocities reported for the Vøring and Møre basins for the Lower Cretaceous and older rocks were also used (Table 3) (Osmundsen and Ebbing, 2008). The velocity analysis to quantify the uncertainty of the depth conversions is included in Supplement 1. The 'best-fit depth conversion' shows good match (±5%) with well tops in the Frøya High and the Rås Basin (Supplement 1). In the deep parts of the basins, where there is a lack of well control, the acoustic basement sits at *c.* 12.7–14.4 km depth. The values reported in the results for faults dip angles, have an uncertainty that increases with depth. For listric faults that flatten with depth, we estimate a maximum uncertainty of ±5° relative to the reported values. We added the geophysical Moho map by Maystrenko et al. (2018) to the depth converted sections (Fig. 5). *Crustal* thinning cannot be reliably calculated, since (i) the geophysical Moho may not match with the lithological Moho (Péron-Pinvidic et al., 2016), and (ii) the Klakk FC's footwall is extensively degraded/eroded. Therefore, the values calculated between the top acoustic basement and geophysical Moho surfaces represent syn-rift *basement* thinning.

Table 1
Basement lithologies drilled by the wells on the Frøya High.

Borehole name	Top depth [m MD*]	Thickness drilled [m MD*]	Lithology description	Rock sample
6306/6-1	1312	5	Dark-grey medium grain crystalline rock	Cuttings
6306/6-2	2072	8	No available	Nine plugs
6407/10-3	2959	14	Fractured granite basement	60 cm core
6407/10-4	3169	55	No available	Eight plugs

MD = Measured depth.

6. Geometry and structure of the Klakk Fault Complex

The down-to-the-west Klakk FC is an N-S non-collinear fault complex composed of several fault segments that delineate two structural salients and two structural recesses (Fig. 4a and c, 4d). The Klakk FC has significant along-strike variability in cross-section, exhibiting overall low-angle, planar to listric geometries with heaves ranging from *c.* 17 km to *c.* 34 km (Figs. 5–9 and Table 4). Post-rift thermal subsidence rotated the Frøya High towards the NW (Bell et al., 2014). Consequently, present-day measured dips represent maximum values and are different from the fault dips during faulting. Fig. 5 shows the fault geometry in the depth domain, while Figs. 6–9 are in the time domain. Although cross-sections A to D are in the depth and time domains and located in the same area (Fig. 4), there is a lateral shift between them (Fig. 4a). The cross-sections in the depth domain focus on the fault geometry and are shifted towards the west, while cross-sections in the time domain show the intra-basement structures in the footwall principally and are shifted to the east.

The central structural salient has a NW-SE trend, while the northern structural salient exhibits an E-W trend (Fig. 4). The central structural salient is a prominent structural feature and shows an arc geometry in map view (Fig. 4b). This salient is *c.* 40 km wide and displays a convex-westwards geometry with a diameter of *c.* 34 km in map view (Fig. 4b). Fig. 4a shows that this arc is highly eroded with the prominent development of canyons that truncates the fault scarp of the Klakk FC. The Klakk FC surrounds this structural salient, and this fault complex changes its strike direction around the salient, from NW-SE in the south west, to NNE-SSW toward the west and to E-W to ENE-SWS towards the north (Fig. 4a). Section C-C′ shows a planar geometry, with dips of *c.* 13° and a minimum heave of *c.* 32 km towards the west of the central structural salient (Fig. 8). The fault scarp on the central structural salient displays a concave-downward geometry, as shown in the dip and strike cross-sections (Fig. 5c and e, 8). The continental crust has a thickness of *c.* 24 km in the footwall and *c.* 11 km in the hanging wall in the central structural salient area (Fig. 5b). We, therefore, calculate a minimum syn-rift basement thinning of *c.* 13 km in the west. The northern salient is *c.* 27 km long and *c.* 17 km wide (Fig. 4a and b and). Two fault segments with an N-S strike connected by a NE-SW fault are localised to the west of the northern structural high (Fig. 4a). Section A-A' shows that the Klakk FC displays a single listric fault plane with a rider block and limited footwall scarp erosion in cross-section (Figs. 5a and 6). The upper part of the fault dips *c.* 44°, shallowing to *c.* 23° with depth and has a minimum heave of *c.* 16.8 km (Fig. 5a and Table 4). The continental crust has a thickness of *c.* 26.4 km on the Frøya High and *c.* 13.5 km in the hanging wall cut-off (Fig. 5a and Table 4). Consequently, we calculated a minimum syn-rift basement thinning of *c.* 13 km to the west in the northern structural salient area (Fig. 5a).

The structural recesses display a significant change in the structural

Table 2
Information of 2D and 3D seismic data used.

Vintage	Type	Area/Length	Total record	IL			XL	
				Rotation from north	Length	Interval	Length	Interval
		[km2]/[km]	[TWT seconds]	[grades]	[km]	[m]	[km]	[m]
ST9302	3D	631.82	6	92	36.8	37.5	21.6	12.5
MC3D-FH2006	3D	1210.51	5	2.5	52.3	12.5	34.7	12.5
CN6306	3D	608.73	6	2.5	40.5	25	19.6	12.5
CE14001	3D	721.29	8	37.8	38.2	12.5	24.5	12.5
SEN1101	3D	695.13	3	91	30	25	30	12.5
SEN1101R15	3D	570.08	3	91	40	25	23.9	12.5
MNR	2D	6225	10					
MC2D-OLE03	2D	2226	9					
MR02-MB	2D	886	7					

configuration in both map and cross-section concerning the structural salients (Figs. 4 and 5). The central structural recess has a convex eastwards geometry in map view, and it cuts *c.* 23 km into the high (Fig. 4a and b and). The central structural recess has an NE-SW eroded ridge that is *c.* 7 km long, which divides the central structural recess into two zones, an inner zone in the eastern flank and an outer zone in the western flank (Fig. 5b). The inner zone has down-to-the-west linked fault segments that change their strike direction from NE-SW to NNE-SSW and are 2–4 km long in map view (Fig. 4d). Cross-section B-B′ shows a down-to-the-west fault with a dip of *c.* 29° and minimum heave of *c.* 2.6 km (Fig. 5b) and may continue as a detachment fault to merge with the outer breakaway zone. This fault bounds a half-graben basin, which shows a sedimentary filling of *c.* 1.4 km thick. Well 6306/5-2 drilled the upper 12 m of this structure and found Upper Jurassic sandstones (Fig. 7). The outer zone has three down to the west linked fault segments with a NE-SW strike and are 10–12 km long in map view (Fig. 4a). In the outer zone, section B-B′ shows that the Klakk FC consists of two interacting fault planes, with dips of *c.* 25° and *c.* 18°, which create a minimum heave of 25.6 km, and an eroded fault scarp of *c.* 5.6 km long (Figs. 4a, 5b and 7). The thickness of continental crust is *c.* 25.3 km in the Frøya High and is *c.* 11.4 km in the Rås Basin (Fig. 5b). Consequently, we calculate a minimum syn-rift basement thinning of *c.* 13.9 km in the west of the central structural recess. The seismic information available for this study allows us to evaluate only the northern part of the southern structural recess (Figs. 2, 4b and 5d, 9). In section D-D', the Klakk FC is a down-to-the-SW fault that strikes NNW-SSE for *c.* 30 km in map view, and it interacts with the fault located to the west of the central structural salient (Fig. 4a). In this cross-section, the Klakk FC has a listric geometry, where the upper part of the fault dips *c.* 44° dip shallowing to *c.* 9° dip with depth, and its scarp is affected by degradation/erosion approximately 4 km into the footwall. We calculate, therefore, a minimum heave of *c.* 20 km. The continental crust is *c.* 24.3 km in the Frøya High and is *c.* 11.9 km in the Rås Basin in cross-section (Fig. 5d). It suggests a syn-rift basement thinning of 12.4 km in the west of this section.

7. Characterisation of the crystalline basement

7.1. Potential fields signature of the Frøya High

The Frøya High is characterised with overall high positive gravity (*c.* 60 mGal) and magnetic (*c.* 1200 nT) anomalies, that do not coincide spatially with each other (Fig. 3). The high positive gravity anomaly is localised above the central structural salient and towards the west of the central structural recess (Fig. 3a). The high gravity anomaly is comprised of three partly overlapping domal anomalies with a clover leaf-like geometry, covering an area of *c.* 40 km × 50 km. In cross-section, the gravity anomalies tend to follow the geometry of the Klakk FC and the Mandel Basin (Figs. 7–9), except in section A-A' where the gravity anomaly has a flat response on the Klakk FC (Fig. 6). Similar high positive gravity values offshore are reported on the Gossa High (*c.* 50 mGal), to the north of the Smøla island (*c.* 60 mGal) and to the west of Molde-Hustad area (*c.* 70 mGal) (Fig. 3a). The high magnetic anomaly is the highest in the mid-Norwegian margin and is located on the northern structural salient and towards the east of the central structural recess (Fig. 3b). It covers an area of *c.* 55 km × 33 km. We do not observe a relationship between the magnetic anomaly and the Klakk FC on cross-sections A to D (Figs. 6–9). Other positive high magnetic anomalies offshore are located towards the north of the Frøya High (*c.* 400 nT) and towards the northeast of the Slørebotn Subbasin (*c.* 300 nT) (Fig. 3b).

Fig. 3 shows the potential field responses in the offshore and onshore areas around the Frøya High. We identify an elongate positive gravity anomaly with a NE-SW direction and *c.* 55 mGal on the CNBW. This anomaly is limited to the south and west by the Høybakken detachment (Fig. 3a). High positive magnetic values are also recorded on Proterozoic crystalline rocks in the western part of the CNBW (*c.* 400 nT) and around the Hustad area (*c.* 300 nT) (Fig. 3b).

7.2. Basement seismic facies

Changes in acoustic impedance, related to lithological or structural heterogeneity can cause local changes in amplitude at depth within the basement (Phillips et al., 2016; Fazlikhani et al., 2017; Lenhart et al., 2019). Although different acquisition and processing parameters in various 2D and 3D seismic surveys produce variations in frequency and amplitude, we used two techniques to identified geophysical artefacts. First, the presence of consistent seismic facies in different surveys located in the same area allows us to separate real reflections from geophysical artefacts with reasonable confidence (Fazlikhani et al., 2017). Second, we converted selected seismic sections to the depth domain (Fig. 5) to identify whether velocities changes caused the intra-basement geometries. These seismic sections preserved the intra-basement geometries, confirming that they are not geophysical artefacts.

We identify five seismic facies (SF1 to SF5) within the footwall of the Klakk FC based on amplitude, internal reflective character, and geometry of intra-basement reflections (Fig. 10).

7.2.1. Seismic facies 1 (SF1)

Observations: SF1 consist of moderately continuous, divergent, subparallel to oblique reflection geometries that have high to medium amplitudes (Fig. 10a). SF1 occurs in the northern part of the southern structural recess, between the Klakk FC and the Mandel Basin (Figs. 9 and 11). The location of this seismic facies coincides with the location of a magnetic low (Fig. 9). The upper boundary of SF1 is the top of the acoustic basement horizon and it passes down into SF4 or SF3.

Interpretation: SF1 shows similar characteristics to the seismic facies defined by Mitchum et al. (1977) for sedimentary rocks. Since no wells have penetrated this seismic facies, the sedimentary affinity of this succession cannot be determined with certainty. SF1 does, however,

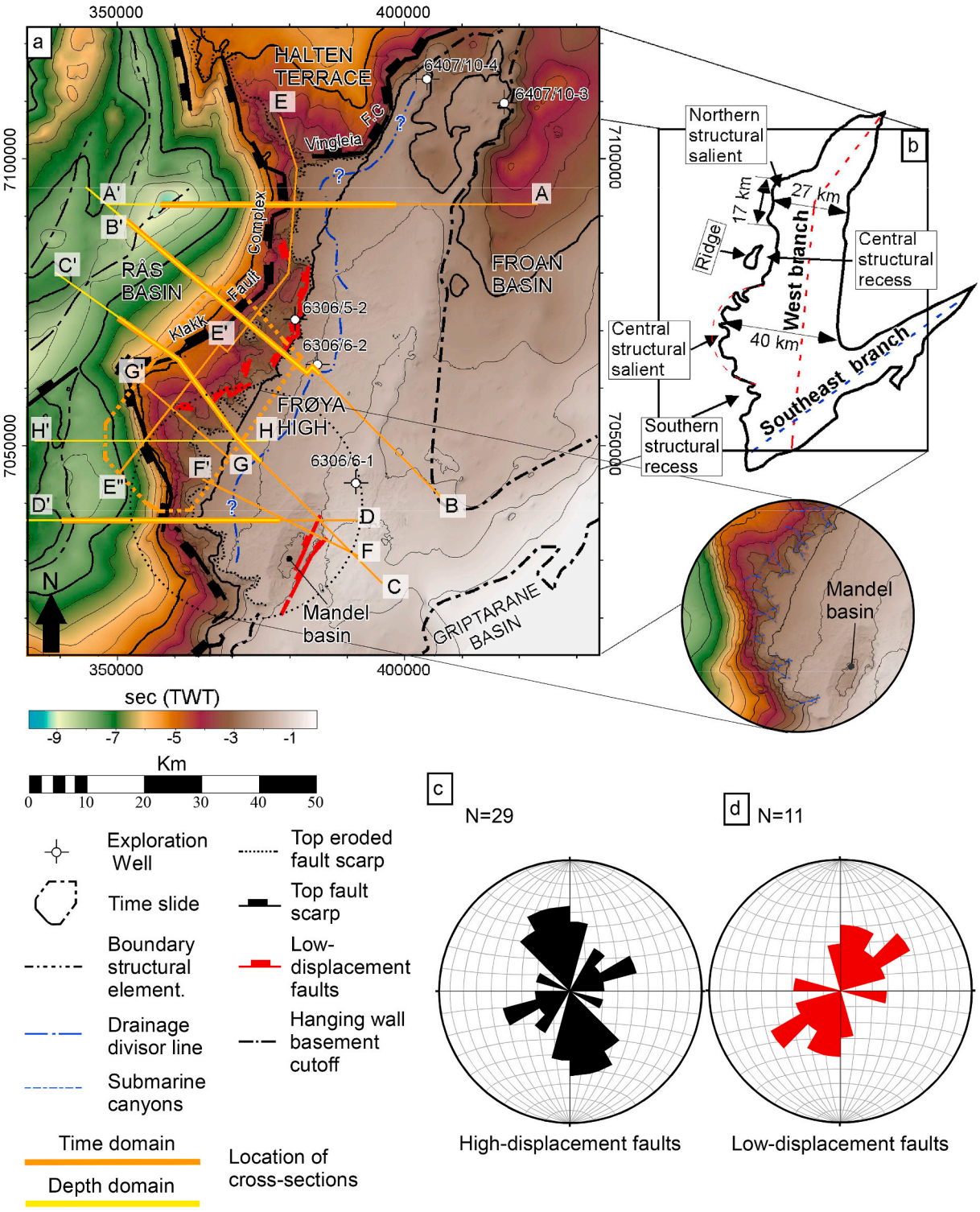

Fig. 4. Structural configuration of the Klakk FC to the west of the Frøya High. (a) TWT structural map at the top of the acoustic basement. Boundaries of structural elements adapted from Blystad et al., 1995. Location on Figure 1a. (b) Morphological geometry of the top acoustic basement on the Frøya High. Rose diagrams showing the strike direction of large-offset fault (c), and low-offset faults (d).

share characteristics and geometries with the intra-basement 'SF1' described by Lenhart et al. (2019) and the 'Seismic Facies 1' described by Fazlikhani et al. (2017), who both suggest that this type of seismic facies likely represent Devonian sedimentary basins.

7.2.2. Seismic facies 2 (SF2)

Observations: SF2 is largely reflection-free with subtle internal areas of low to medium amplitude discontinues to chaotic reflections (Fig. 10b). SF2 occurs in the central and northern part of the Frøya High in map view, and it tends to die-out to some reflection of SF3 to the west (Figs. 6–8). The upper boundary of SF2 is the top of the acoustic basement reflection and it passes downward into SF4 in the central and west part of the Frøya high in map view. Boreholes 6306/6-1 and 6306/6-2 penetrate SF2 reporting rocks of granitic composition (Fig. 4a and

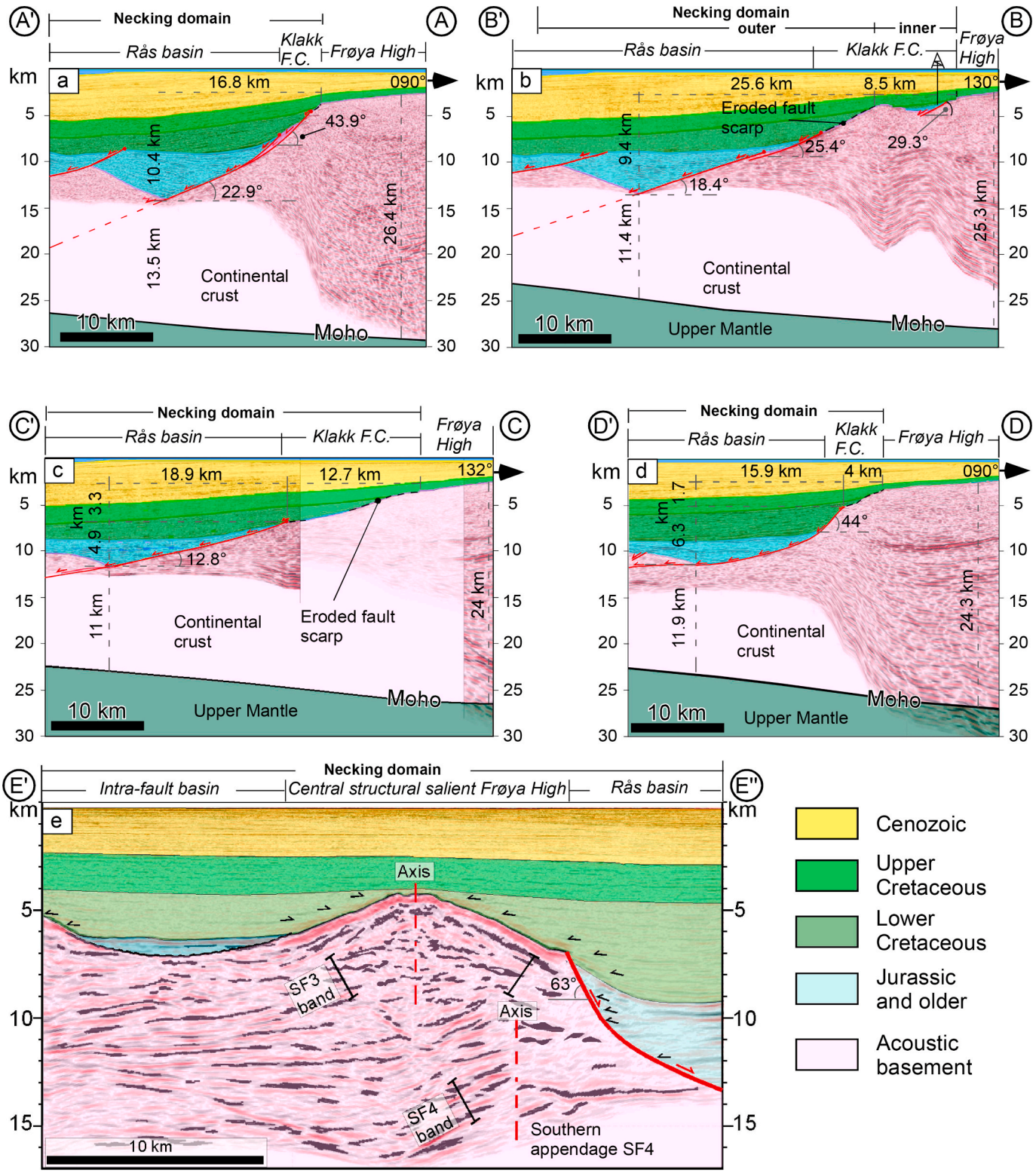

Fig. 5. Fault segments geometries in the Klakk FC and variation along strike in depth domain. Fig. 4 shows the location of cross-sections in depth domain (yellow lines). (a) Cross-section along dip direction to the west of the northern structural salient. (b) Cross-section along dip direction between the northern and central structural salients. (c) Cross-section along dip direction to the west of the central structural salient. (d) Cross-section along dip direction towards the south of the central structural salient. (e) Cross-section along strike direction above the central structural salient. Seismic sections without interpretation in Figs. 6a, 7a, 8a, 9a, 15. Velocity sensitive analysis for depth conversion is shown in supplement 1. (For interpretation of the references to colour in this figure legend, the reader is referred to the Web version of this article.)

Table 3
Velocities used for depth conversion and comparison with other regional study.

Unit	Osmundsen and Ebbing. (2008)		This work
	Terrace	Deep basin	
	(m/s)	(m/s)	(m/s)
Seawater	1450	1450	1450
Cenozoic	1800–2400	1800–2400	2100
Upper Cretaceous	2400–3200	2700–3600	2650
Lower Cretaceous	2800–3200	3600–5000	4300
Jurassic	3200–3750	5000–6000	5500
Triassic	4250–5000	5000–6000	6000
Palaeozoic	–	5000–6000	6000
Continental crust	6000–6500	6000–6500	6000

Table 1).

Interpretations: The 6306/6-1 and 6306/6-2 wells reported weathered granite rocks. SF2 coincides with the location of the irregular oval-like positive magnetic anomaly. This high magnitude anomaly has been interpreted as uplifted highly magnetic Precambrian granitic to granodioritic rocks (Skilbrei et al., 2002; Skilbrei and Olesen, 2005; Maystrenko et al., 2018). We, therefore, interpret SF2 as a lithological unit, related to the exhumed Baltic basement.

7.2.3. Seismic facies 3 (SF3)

Observations: SF3 comprises moderate to high amplitude reflections with overall semi-continuous braided to inclined geometries gathered in tabular bands (Figs. 10c and 6 to 9). SF3 generally features antiformal shapes in the immediate footwall of the Klakk FC between 3.0 and 5.5 s TWT (Figs. 6–9). The upper and west boundary of SF3 is the eroded fault scarp or top of the acoustic basement; the east boundary is the SF2, and SF3 passes down into SF4.

Interpretation: SF3 has not been penetrated by wellbores. Although SF3 has not been described as an intra-basement seismic facies in other publications, similar reflection geometries have been reported in the Norwegian Sea, Uruguay, the Barents Sea, the North Sea, Vietnam and New Zealand, where they have been interpreted as rift-related shear zones (Osmundsen and Ebbing, 2008; Peron-Pinvidic et al., 2013; Clerc et al., 2015, 2018; Osmundsen and Péron-Pinvidic, 2018; Henstra et al., 2019; Phillips and McCaffrey, 2019). We interpret that the SF3 corresponds to shear zones related to the high-displacement faults (thinning phase) based on the location and the similarity with rift-related shear zones. We observe that SF3 is not connected with SF4 (Figs. 4 and 14, 15). This observation leads us to the interpretation that these seismic facies are not related to one and the same structure. We discuss this in section 8.1.3.

7.2.4. Seismic facies 4 (SF4)

Observations: SF4 is characterised by high to very high amplitude grouped together in tabular bands with continuous reflections that have internal multiple inclined or converging geometries (Figs. 10d and 6 to 9). The tabular bands of SF4 are 0.5–1.5 s thick and tend to generate a major anticline towards the east of the central structural salient and central and southern recesses (Figs. 7–9). The upper boundary of SF4 is SF1, SF2 and SF3. In some places, SF4 mixes or merges with SF3. SF4 passes gradually down into SF5.

Interpretation: SF4 is similar to 'Seismic facies 2′ of Fazlikhani et al. (2017), 'SF3' of Lenhart et al. (2019) in the northern Viking Graben, which are inferred to be associated with Devonian shear zones. In addition, SF4 has similar characteristics and geometries to the Palaeozoic detachment interpreted by Osmundsen et al. (2002) below the Vingleia Fault Complex and Trøndelag Platform (Fig. 2). The three papers mentioned above all suggest that these Devonian shear zones are a continuation of onshore shear zones generated during the orogenic collapse of the Caledonian orogen. Based on the seismic facies similarities, the location and the presence of Devonian shear zones in the area, we propose that SF4 represents an inherited Devonian shear zone.

7.2.5. Seismic facies 5 (SF5)

Observations: SF5 occurs in the deepest part of the seismic data, generally below the six to 7 s TWT, and it composed of high amplitude discontinuous to chaotic reflections (Figs. 6–9).

Interpretation: This seismic facies is similar to 'SF4' of Lenhart et al. (2019), who suggest it is representing the Baltic basement. We therefore suggest that SF5 represents the lower continental crust, which is composed of reworked Baltic basement similar to the exhumed basement in the WGR or CNBW (Braathen et al., 2000; Osmundsen and Andersen, 2001; Osmundsen et al., 2006; Fossen, 2010; Andersen et al., 2012; Corfu et al., 2014; Fossen et al., 2016).

7.3. Geometry of intra-basement reflective packages

Three distinct intra-basement structures have been identified based on the geometry of reflections and arrangement of seismic facies: (i) a bowl-shaped structure that contain the SF1 seismic facies, (ii) a hyperbolic structure associated to SF4 reflectivity, and (iii) a dome structure generated for SF3 reflections in the immediate footwall of the Klakk FC (Figs. 11–15).

7.3.1. Bowl-shaped structure related to SF1

A bowl-shaped structure below the immediate acoustic top basement has a WNW-ESE direction and an area of *c.* 25 km × 22 km (Fig. 11). This structure is located in the west of the Frøya High, between the central structural salient and southern recess (Fig. 11a). The spoon-shaped structure contains reflections of SF1 and is *c.* 12 km long and *c.* 0.36 s TWT thick (*c.* 1 km) in section F-F' (Fig. 11c). The basin has depositional contact with the top basement reflection. The band with SF4 has a ramp-flat-ramp geometry *c.* 6.5 s TWT below the spoon-shaped structure. The seismic facies in this structure differs from seismic facies in the Mandel Basin. SF1 shows an oblique geometry, while in the Mandel Basin, reflections are high amplitude, high-frequency with continues and parallel geometries that are truncated by Jurassic sedimentary strata (Fig. 11b and c and).

7.3.2. Hyperbolic surface belonging to SF4

Poor continuity, overprinting and braided internal geometries in seismic reflections of SF4 package make challenging to do a single structural map (Figs. 6–9 & 12, 14, 15). In addition, the 3D seismic reflection data do not cover the structure with deep enough. To solve this issue, we created different structural maps at the top of SF4 of the same reflection packages (Fig. 13a) and chose the most common geometry of these maps (Fig. 13b).

A very strong, high amplitude tabular band with reflections of SF4 appears in cross-sections A to D between 4 and 8 s TWT (Figs. 6–9 & 12a) and in the time slices on the central structural salient (Fig. 12b). In section A-A′, SF4 display two asymmetric tight anticlines structures separated by a major syncline structure. The axes of these anticlines coincide with the location of the westernmost part of the Froan Basin and the Klakk FC (Fig. 6a and c and). The band of SF4 forms three similar structures in sections B-B′, C-C′ and D-D': an asymmetrical anticline towards the east, a flat to gently west-dipping area to the west, and west-dipping monocline below the Klakk FC (Figs. 7–9). In section B-B′, the asymmetrical anticline is *c.* 19 km long, the gently west-dipping structure is *c.* 14.5 km long, and a small asymmetrical anticline below the ridge is *c.* 16 km long (Fig. 7). In section C-C′, the asymmetric anticline has *c.* 40 km long, the flat zone of *c.* 9 km long, and the NW-dipping monocline is *c.* 8 km long below the Klakk FC strand (Fig. 8a and c and). In section D-D′, the anticline is *c.* 22.4 km long, the flat area is *c.* 10.5 km long and the monocline *c.* 10 km long. SF4 forms an NW-plunging tight anticline on the central structural salient (Figs. 5e and 12), and a west-plunging anticline on the central structural recess (Figs. 5e and 12a and). Tabular bands with reflections of SF4 appears

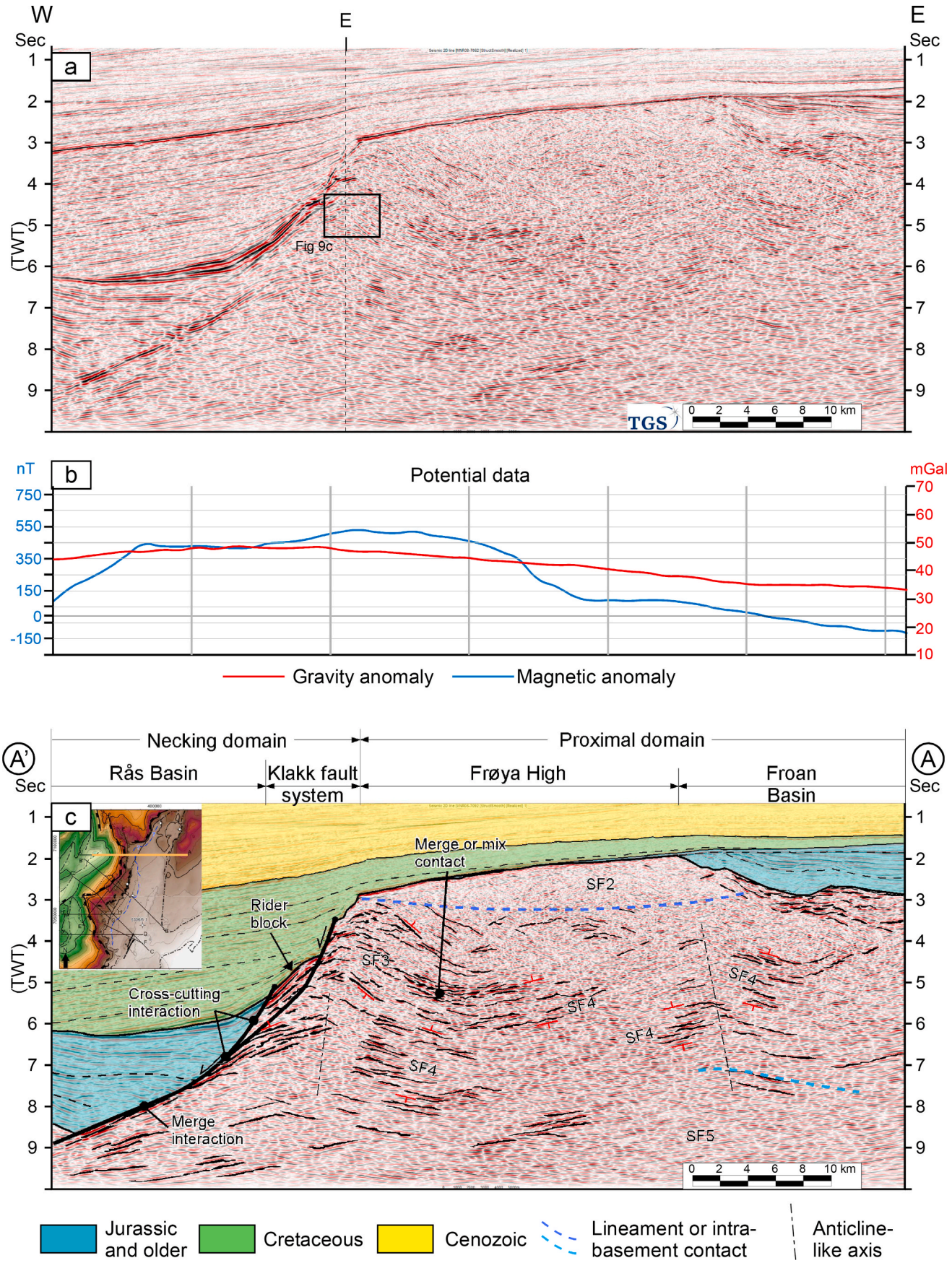

Fig. 6. Cross section A-A' at the northern structural salient. (a) Composite seismic sections without interpretation. (b) Potential data profiles. (c) Seismic section interpreted.

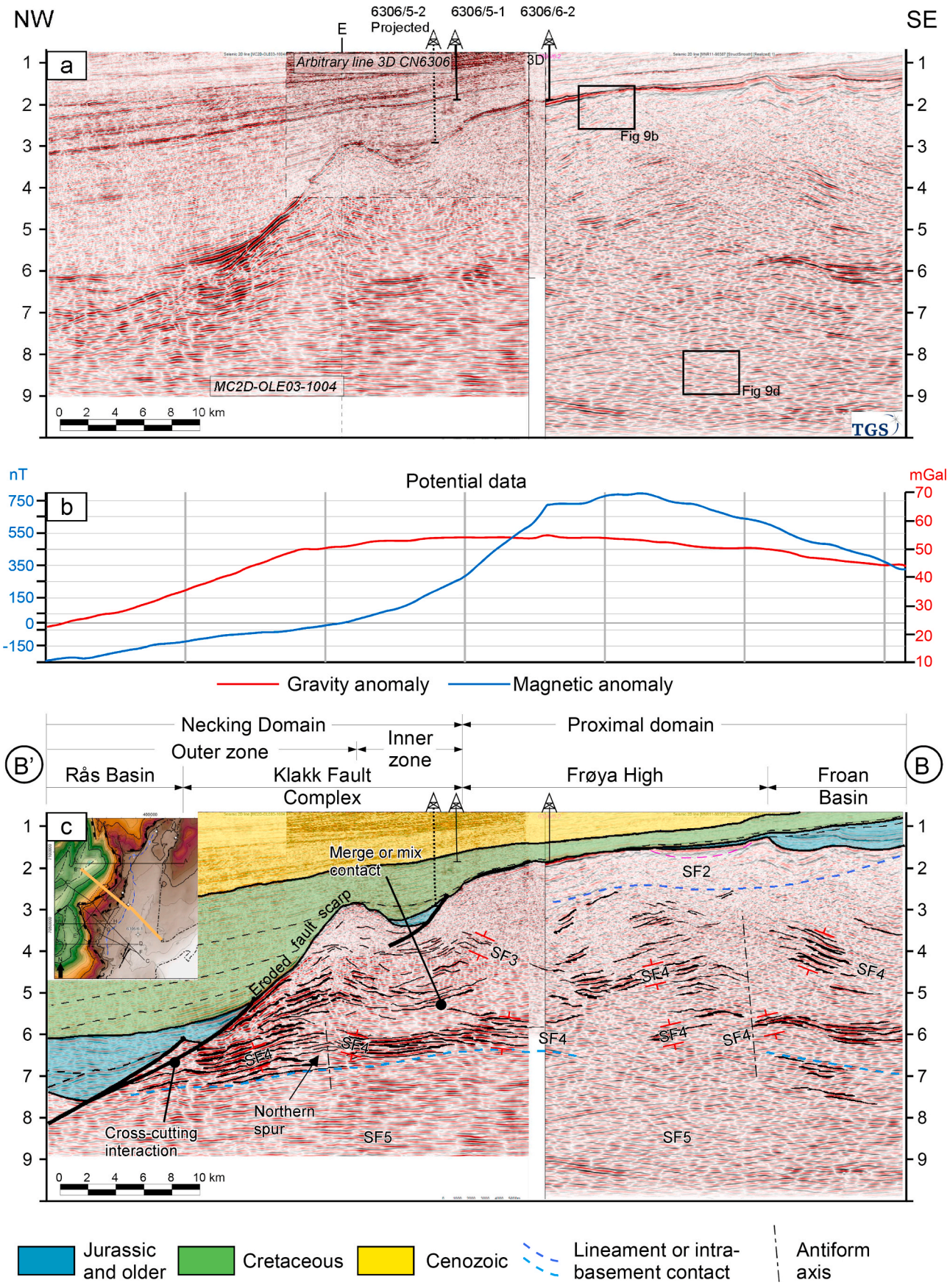

Fig. 7. Cross section B-B' at the central structural recess. (a) Composite seismic section without interpretation. (b) Potential data profiles. (c) Seismic section interpreted.

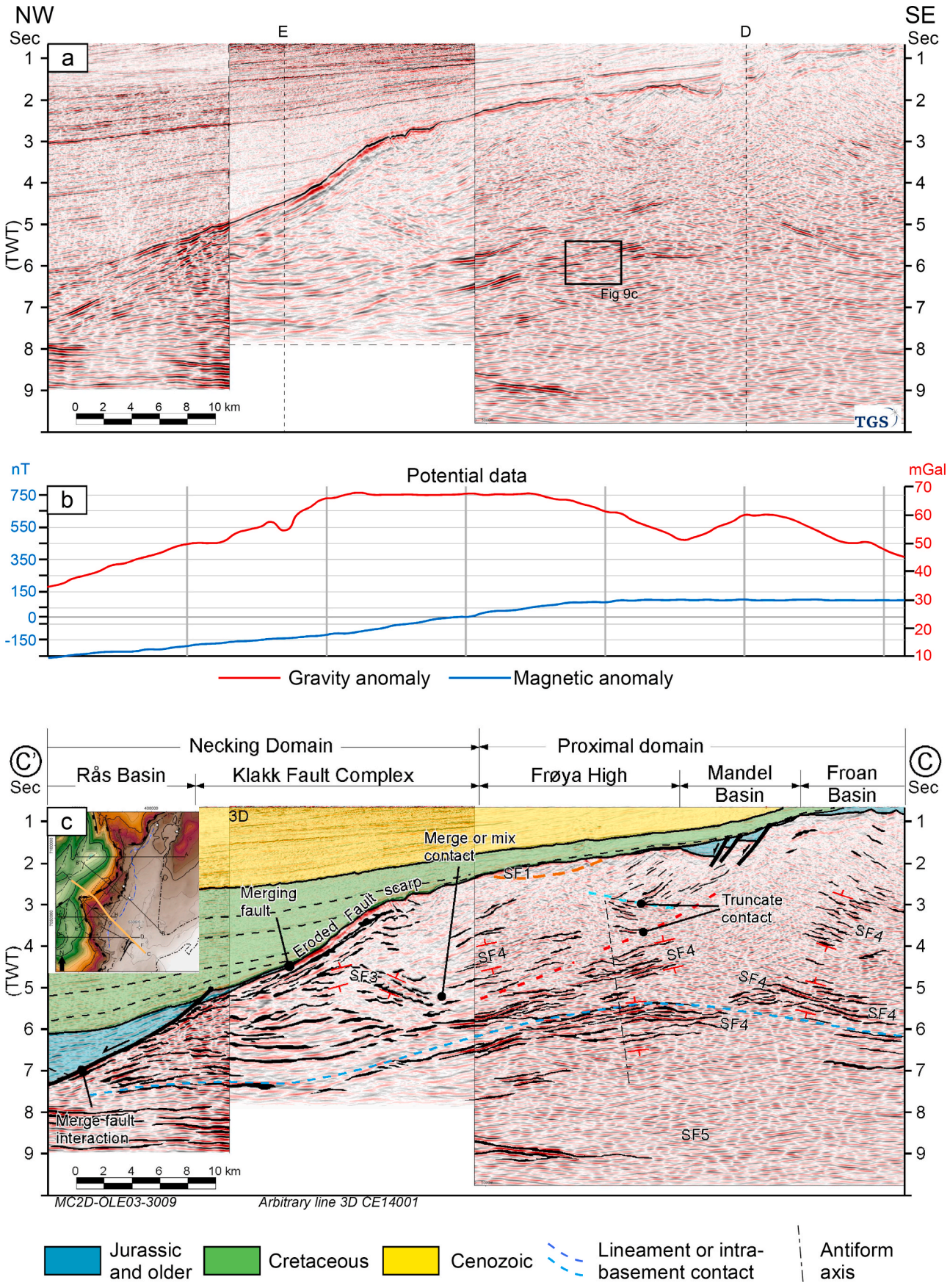

Fig. 8. Cross section C-C' at the central structural salient. (a) Composite seismic section without interpretation. (b) Potential data profiles. (c) Seismic section interpreted.

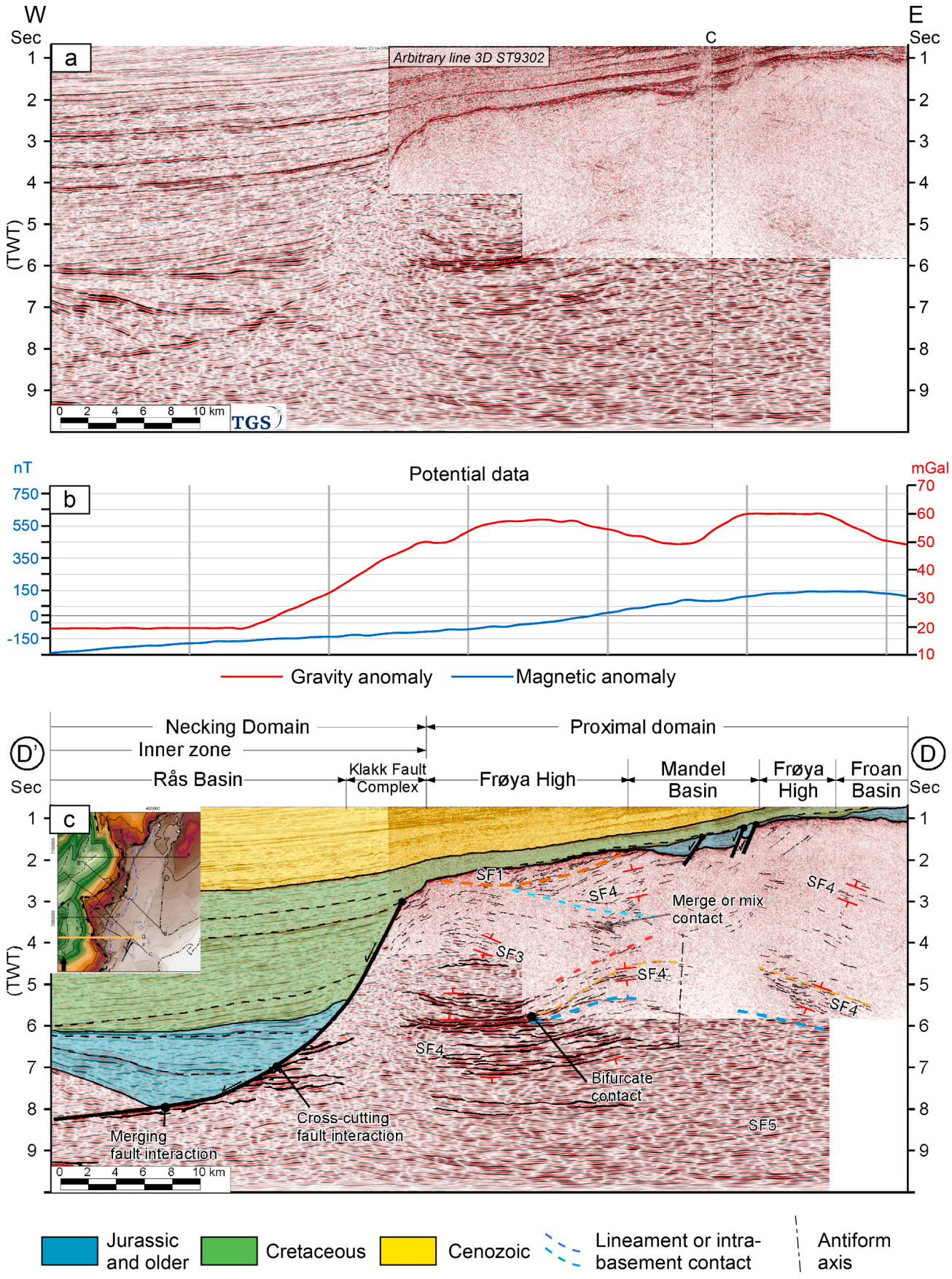

Fig. 9. Cross section D-D'. (a) Composite seismic section without interpretation. (b) Potential data profiles. (c) Seismic section interpreted.

Table 4
Characterisation of the segments that compose the Klakk Fault Complex at the structural cross-sections A to D.

Section	Zones	Heave	Throw	Displacement	Angles		Lateral length of eroded fault scarp
					At top fault scarp	At hanging wall cut-off	
		[km]	[km]	[km]	[Degree]	[Degree]	[km]
A-A′	Single	17	10	19.8	44	23	1.3
B-B′	Inner	1.5	0.9	2.2	34.5	28	1.2
B-B′	Outer	25.4	9.5	27.5	6.2	28.3	18.3
C-C′	Single	31.6	8.2	34.4	24	13	15
D-D′	Single	20	8	22.2	48	1.8	4.5

upwards until *c.* 3 s TWT (Figs. 6–9 & 12). Consequently, the Klakk FC shows a cross-cutting interaction (sensu Phillips et al., 2016) with SF4 until *c.* 6.5–7.2 s TWT, where it changes to a merging interaction (sensu Phillips et al., 2016) around the band of SF4 referenced (Figs. 5e, 6c and 8c, 9c). Locally, the Klakk FC exhibits a ramp-flat-ramp cross-sectional fault geometry (cf. Rotevatn and Jackson, 2014) where the fault overall cross-cuts the SF4 fabric, but locally merges with and follows the SF4 along the 'flat' (Fig. 12a).

The SF4 surface is best described as a west-dipping hyperbolic surface in three-dimensions which is composed by domes, antiforms and saddles that vary along and across strike (Fig. 13). These antiforms and saddles show two trends, parallel and perpendicular to the extension direction, and with an WNW trending through dividing the surface into two areas (Fig. 13b). The southern area shows an N-S elongate dome, which is *c.* 59.5 km long and *c.* 49 km wide at 6 s TWT. The geometry of this structure, however, changes at *c.* 6.4 s TWT depth, where it becomes a NW-plunging antiform towards the west. We name this antiformal structure as the "southern spur", which is *c.* 25 km long at 7.5 s TWT (Fig. 13b). The northern area displays two antiformal and one domal structures above 6.4 s TWT. At 6 s TWT, "antiform 1" strikes NNE-SSW and is > 26.6 km long, "antiform 2" strikes E-W to NE-SW and is > 39 km, and "dome C″ is *c.* 11 km "Antiform 2″ continues to the west forming the 'northern spur', which is *c.* 29 km long, *c.* 27.6 km wide at 7.4 s TWT (Fig. 13b). The interpretation of the structures, located to the north of the WNW depression, has significant uncertainty because of the poor continuity of the SF4 reflections (Fig. 13b).

The SF4 west-dipping hyperbolic surface geometry correlates well with the cloverleaf geometry observed in the gravity anomaly map (Fig. 13c) and the structural map at the top of the acoustic basement (Fig. 13d). Both the SF4 structure and gravity anomaly values dip toward the west, and the southern and northern spurs of SF4 overlap with the NW cloverleaf gravity anomaly (Fig. 13c). Moreover, we identify that the top of the eroded fault scarp of the Klakk FC coincides with the western flank of the gravity anomaly (Fig. 13c). Fig. 13d shows that the southern spur of SF4 matches with the central structural salient, while the northern spur of SF4 matches with the ridge located in the central structural recess. The Klakk FC is localised towards the western flank of both the gravity and SF4 structures (Fig. 13c and d and). The segments of Klakk FC with displacement <3 km are localised in the eastern part of the central structural recess, which matches with the geometry of the SF4 spurs in this area. In addition, the basement map shows a series of west-trending canyons that coincide with the structural saddles located between the southern spur, north spur and northern structural salient (Fig. 13d).

7.3.3. Domal structure associated with SF3

A concave-downward tabular band of SF3 reflections form an elongate domal intra-basement structure in the westernmost part of the central structural salient at 4–5.5 s TWT (Figs. 5e, 14 and 15). The structure exhibits a series of sub-domes within a tabular band of *c.* 1.5 s TWT (Figs. 5e, 14a and 15), which is manifested as a circular geometry of *c.* 5 km diameter in a time slice at 4.5 s TWT (Fig. 12b). The long axis of the dome structure is tilted to the SE in the dip direction, similar to the slope of the eroded fault scarp of the Klakk FC (Fig. 14a). The dome is located into the immediate footwall below the Klakk FC eroded fault scarp, and it interacts with the Klakk FC in an acute cross-cutting contact (Figs. 5e, 14a and 15).

The dome structure overprints the southern spur of SF4. The dome structure is located above a continuous tabular band of SF4 that dips towards the west in the dip direction (Fig. 14a), whereas at 5.5 s TWT (*c.* 10 km), this structure is separated by 5 km from the axis of the SF4 anticline in the strike direction (Figs. 5e and 15 and). At 4.5 s TWT, the time slice shows two structures, a circular structure with SF3 at the NNW in the central structural salient and an NW-plunging anticline with SF4 in the SW part of the central structural salient (Fig. 14b). The absence of SF3 structures below 6.5 s TWT, the separation between the axes of SF3 dome and SF4 southern spur, and the presence of both structures at 4.5 s TWT suggest that SF3 dome overprinted the SF4 southern spur.

8. Discussion

8.1. Interpretation of the intra-basement structures

We discuss the nature of the three intra-basement structures identified based on (i) the character of the intra-basement seismic facies, (ii) the location and geometry of the seismic facies, (iii) the geometries of the structures identified and (iv) the correlation with nearby intra-basement structures that are described in the literature (e.g. Osmundsen et al., 2002; Phillips et al., 2016; Fazlikhani et al., 2017; Lenhart et al., 2019).

8.1.1. Devonian sedimentary basin

A bowl-like geometry structure gathers the SF1 facies, which we interpret as a Palaeozoic, likely Devonian (?), sedimentary basin (Fig. 11a); the basis for this interpretation is laid out below. The basin is located immediately below the top of the acoustic basement and above the ramp-flat-ramp geometry of SF4 band at *c.* 6.5 s TWT (Figs. 9 and 11). In addition, we observe a depositional contact between the Devonian (?) sedimentary rocks and the underlying (likely) crystalline or metamorphic basement. Devonian sedimentary basins outcrops towards the west of the study area ('Old Red Sandstones') (Braathen et al., 2000; Eide et al., 2005), and have been proposed in the offshore in the northern Viking graben (Fazlikhani et al., 2017; Lenhart et al., 2019). In addition, the Devonian Håsteinen basin in onshore Norway has been interpreted as a ramp-type basin, which is related to the ramp-flat-ramp geometry of the Nordfjord-Sogn Detachment Zone (Vetti and Fossen, 2012). Supported by the regional prominence of Devonian sedimentary basins, our observations lead us to interpret this basin as a Devonian supra-detachment ramp-type basin (sensu Vetti and Fossen, 2012). Our interpretation aligns with the observations of Trice et al. (2019), who propose a Devonian or Carboniferous basin in the acoustic basement using broadband reprocessed seismic data in the same geographical area where we identify the SF1.

8.1.2. SF4 shear zone as an offshore extension of the Devonian Høybakken Detachment

The SF4 shear zone identified in the southern Frøya High has the same hyperbolic geometry as other Devonian detachment geometries

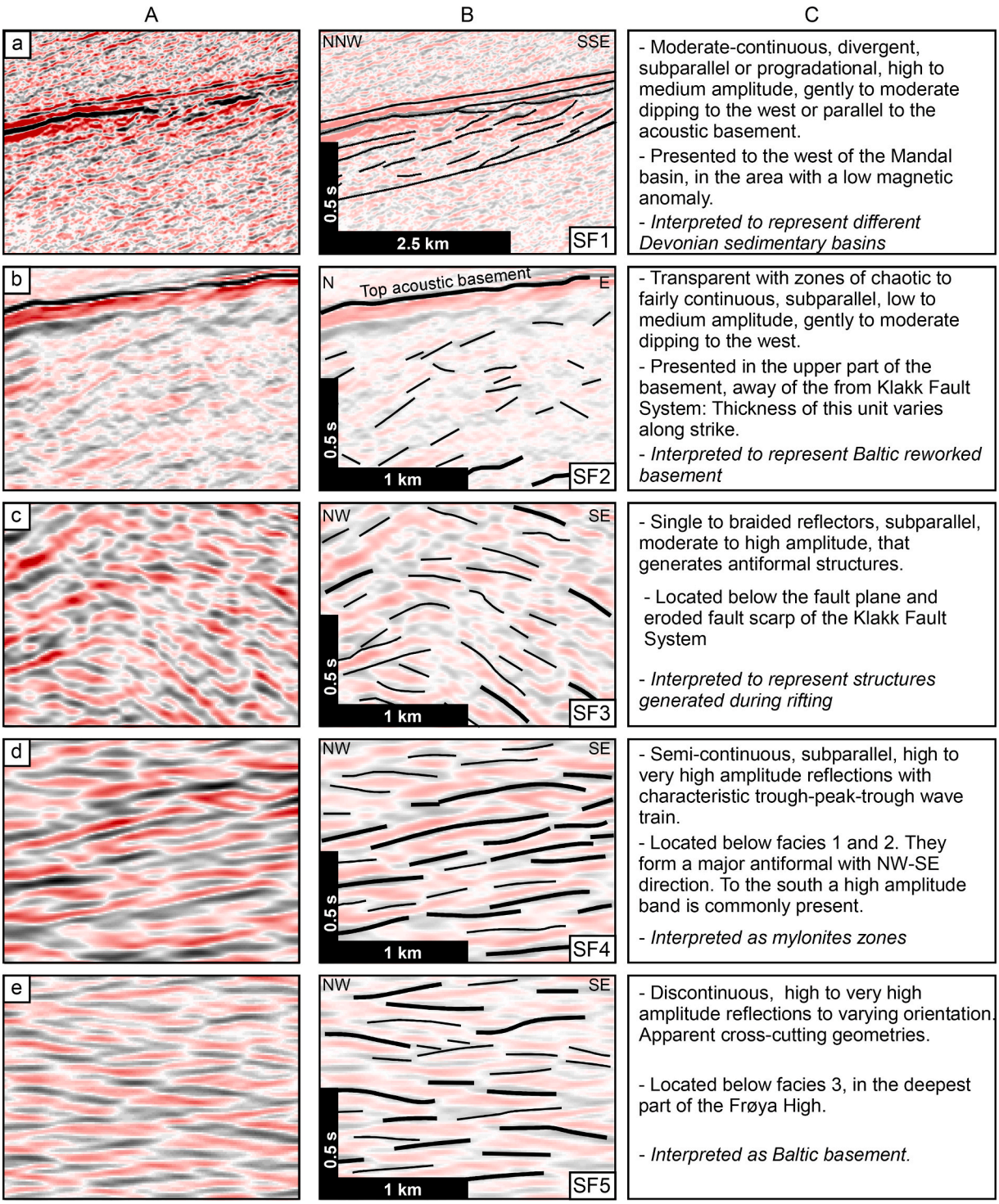

Fig. 10. Seismic facies (SF1-SF5) based on the intra-basement reflections on the Frøya High. Column a: uninterpreted section. Column b: interpreted section. Column c: description and interpretation. Location at Figs. 6-8 & 11.

mapped onshore and offshore Norway. The SF4 shear zone shows a ramp-flat geometry in a dip-direction cross-section, which is similar to the one below the Vingleia Fault in cross-section (Figs. 6–9 & 12) (Osmundsen et al., 2002, 2016; Osmundsen and Péron-Pinvidic, 2018). In three-dimensions, the SF4 shear zone shows a complex west-dipping hyperbolic structure (sensu Wiest et al., 2019) comprised of anticlines, domes and spurs similar to the Nordfjord-Sogn Detachment Zone or the Høybakken Detachment onshore Norway (Figs. 15, 16a and 16c) (Osmundsen et al., 1998, 2002, 2006; Braathen et al., 2000; Skilbrei et al., 2002; Fazlikhani et al., 2017; Lenhart et al., 2019). Using potential field data, Skilbrei et al. (2002) propose that the Høybakken, Kollstraumen and Nesna detachments extend offshore with an NW to NNW-strike direction (Fig. 3). In addition, Osmundsen et al. (2002) interpret that the detachment zone underneath the Vingleia Fault Complex may correspond to the offshore extension of the Høybakken detachment on the Frøya High. Mjelde et al. (2016) suggest that the JML is a detachment zone that joins the MTCF in the southern Frøya High. The SF4 shear zone mapped in this study coincides with the

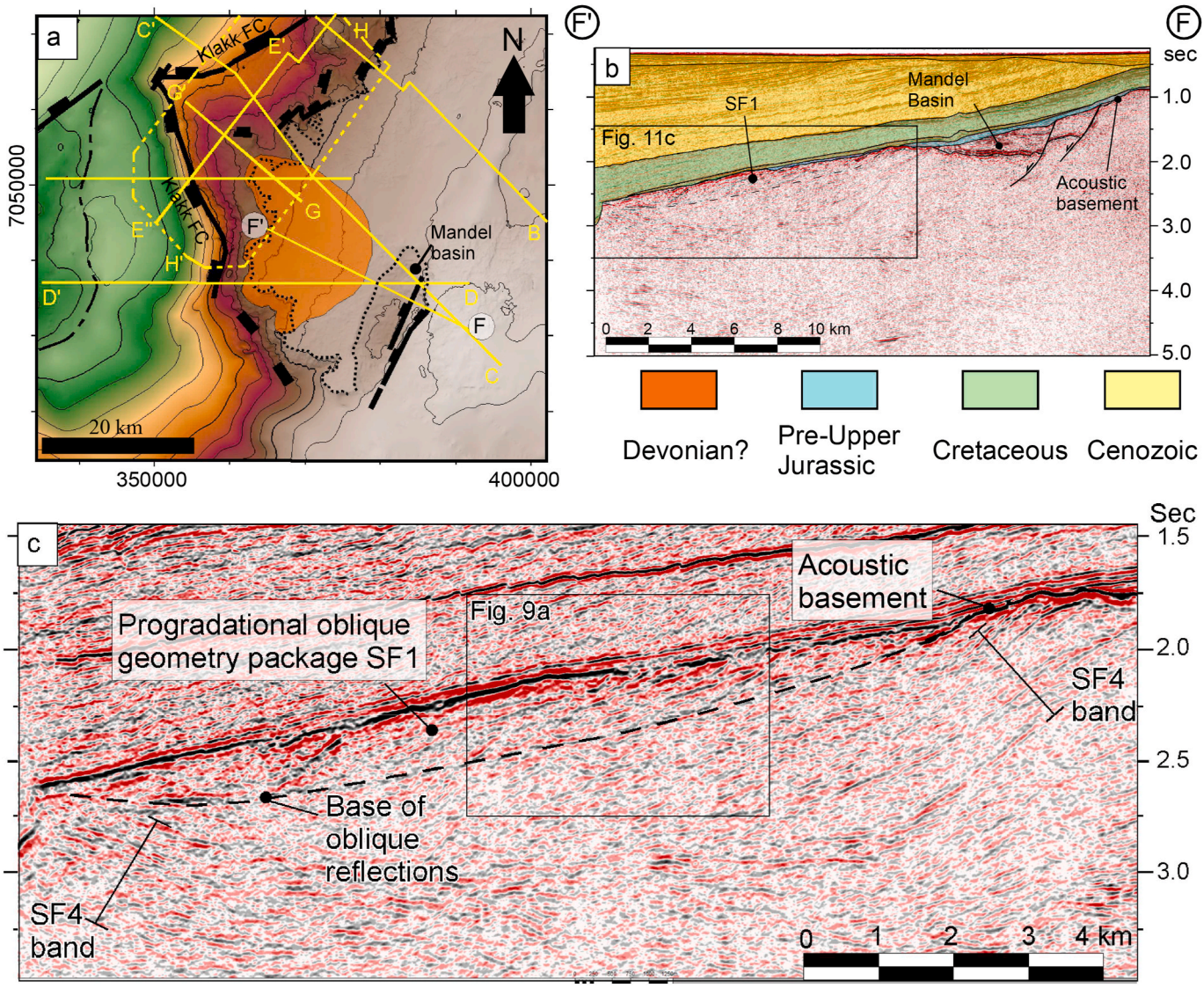

Fig. 11. Spoon-shaped basin into the Frøya High. (a) Location of the basin and its relationship with Klakk FC in map view, (b) geometry and position of the basin in cross-sectional view, (c) zoom showing the internal geometries of SF1 that fill the basin.

southernmost location of the detachment zone proposed by Mjelde et al. (2016). Instead of joining the JML, however, the shear zone mapped in this study has NNE-SSW strike direction at 6 s TWT. This pattern coincides with the location of the central structural salient and the ridge in the central structural recess. Also, the presence of a series of anticlines above 6 s TWT, where the east flank localises toward the Froan Basin, may suggest that SF4 shear zone is the westward continuation of the Høybakken detachment.

Fig. 8 by Gernigon et al. (2020) shows high-velocity lower crustal bodies that coincide with the geometry of our SF4 shear zone in the north and northwest parts of the Frøya High. The 'high-velocity lower crust' (also termed 'lower crust body' in Gernigon et al., 2020) has been interpreted as, (i) gabbroid intrusions into the pre-existing continental crust during the continental breakup, or (ii) inherited eclogites bodies (Gernigon et al., 2003; Mjelde et al., 2005, 2013). These bodies show velocities of 7.3–7.6 km/s, and they were identified initially in the distal and outer domains of rifted margins (Gernigon et al., 2003; Mjelde et al., 2005, 2009a, 2009b, 2013). The high-velocity lower crustal bodies tend to thin and occur at progressively deeper levels towards the proximal domain. The hyperbolic geometry of SF4, however, show a series of intra-basement antiformal structures towards the top of the crystalline basement. We, therefore, suggest that the intra-basement reflections interpreted in Fig. 8 by Gernigon et al. (2020) are part of the same inherited shear zone as that which we correlate to SF4.

8.1.3. A rift-related shear zone and continental margin core complex

We interpret the SF3 symmetrical anticline as a shear zone related to rifting. The high-displacement of the Klakk FC has been related to the late Jurassic and early Cretaceous rifting phases (thinning and hyper-extension deformation phases) (Blystad et al., 1995; Doré et al., 1999; Faleide et al., 2010; Péron-Pinvidic and Osmundsen, 2018). Peron-Pinvidic et al. (2013) describe that high-β 'type 1' faults generated during the thinning deformation phase may create rift-related shear zones in the necking domain. Osmundsen et al. (2002) and Osmundsen and Péron-Pinvidic (2018) show similar reflections to SF3 underneath the Gossa High, which is located *c.* 62 km towards the SSW of the central structural salient (Fig. 2). They propose that these reflections correspond to the Slørebotn detachment, generated because of the displacement of the outer fault of the Møre-Trøndelag Fault Complex during the late Jurassic and early Cretaceous rifting phases. We interpret that the dome structure of SF3 on the NW-most part of the central structural salient is a rift-related shear zone because of the displacement of the Klakk FC and footwall isostatic compensation. The SF3 shear zone overprinted reflections of SF4 and might have formed at the same time as the Slørebotn

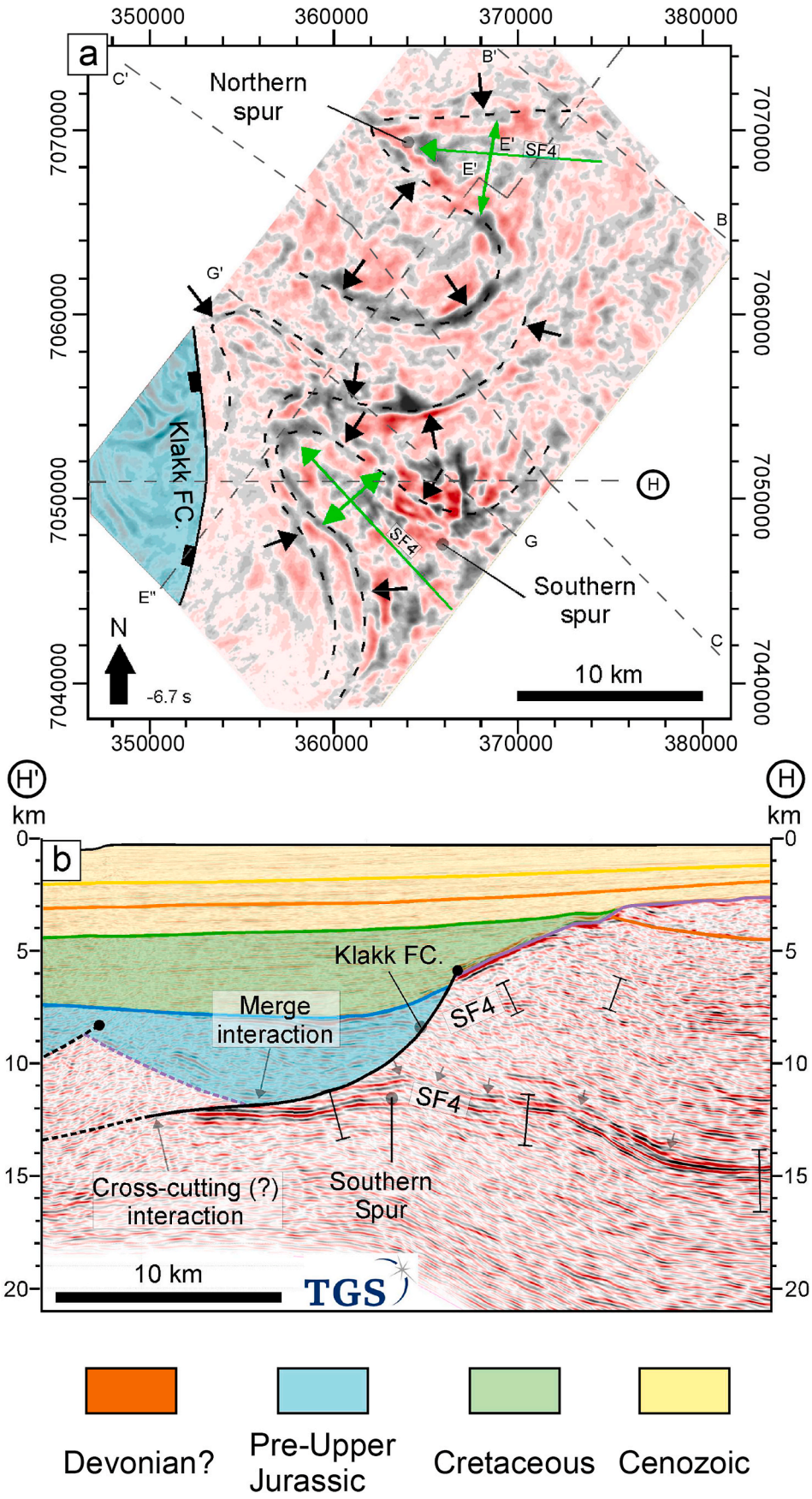

Fig. 12. Geometry of the SF4 band on the central structural salient and recess. a) Cross-section in depth showing the geometry of the SF4 band and the relationship with the Klakk FC. b) Time slice showing the 3D geometry of the southern and northern spurs of SF4.

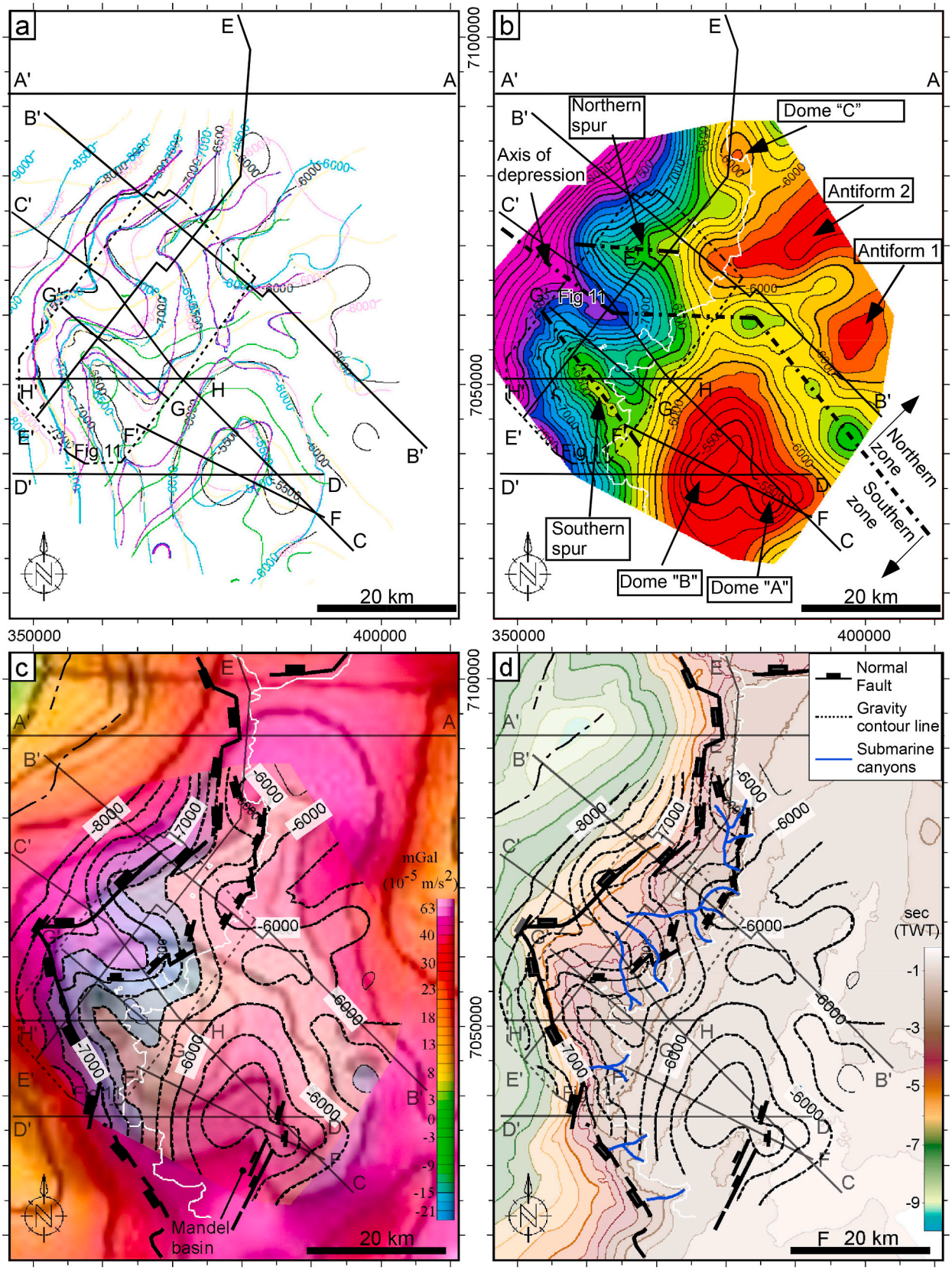

Fig. 13. Structural map of SF4 and relationship with gravity anomaly data and Klakk FC. (a) Seven interactions for mapping of this band (seconds TWT). (b) Best fit structural map (seconds TWT). (c) Comparison between structural map of Fig. 12b with density anomaly map (Fig. 3a). (d) Comparison between structural map of Fig. 13b with top of basement map (Fig. 4a).

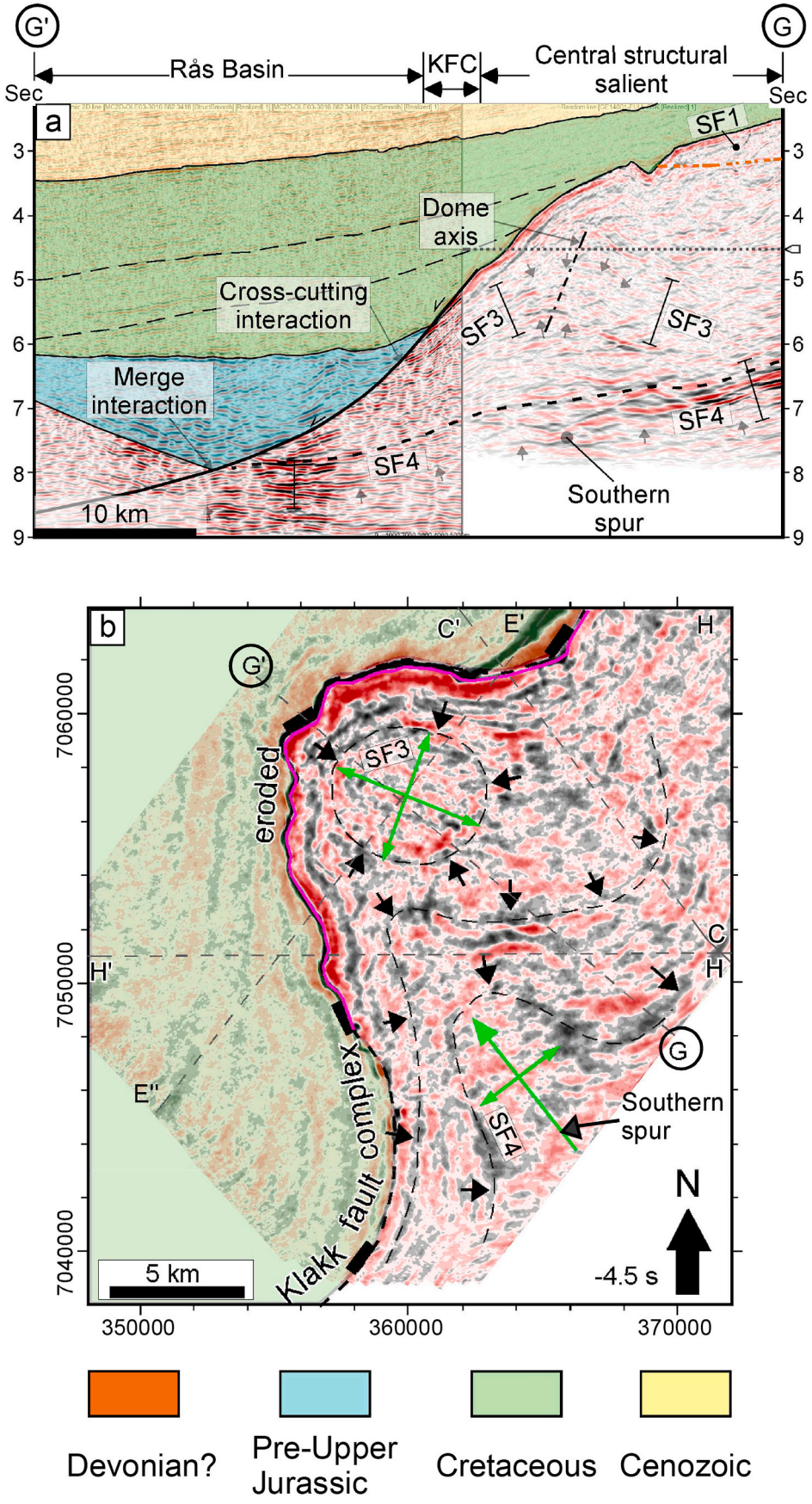

Fig. 14. Intra-basement dome structure in the western most part of the structural salient. (a) cross-section in the dip direction and (b) time slice at 4.5 s. Fig. 15 shows this intra-basement structure in cross-sections in the strike direction.

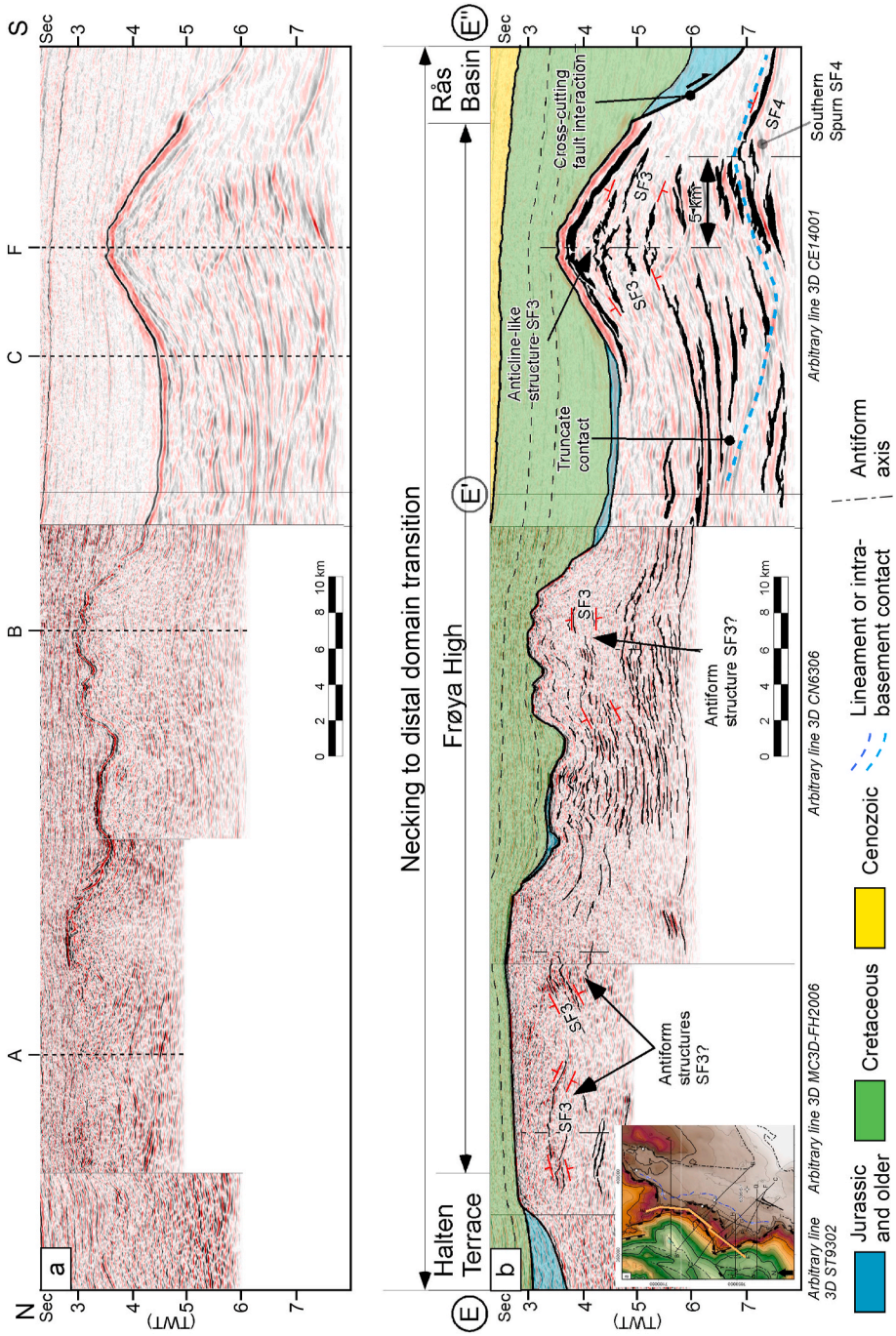

Fig. 15. Cross section E-E′ along strike of the inner part of the Klakk Fault Complex. (a) Composite seismic section without interpretation. (b) Seismic section interpreted. E′-E″ shows the relationship between SF4 and SF3 in strike direction. Fig. 5e shows this part of the cross-section in depth domain.

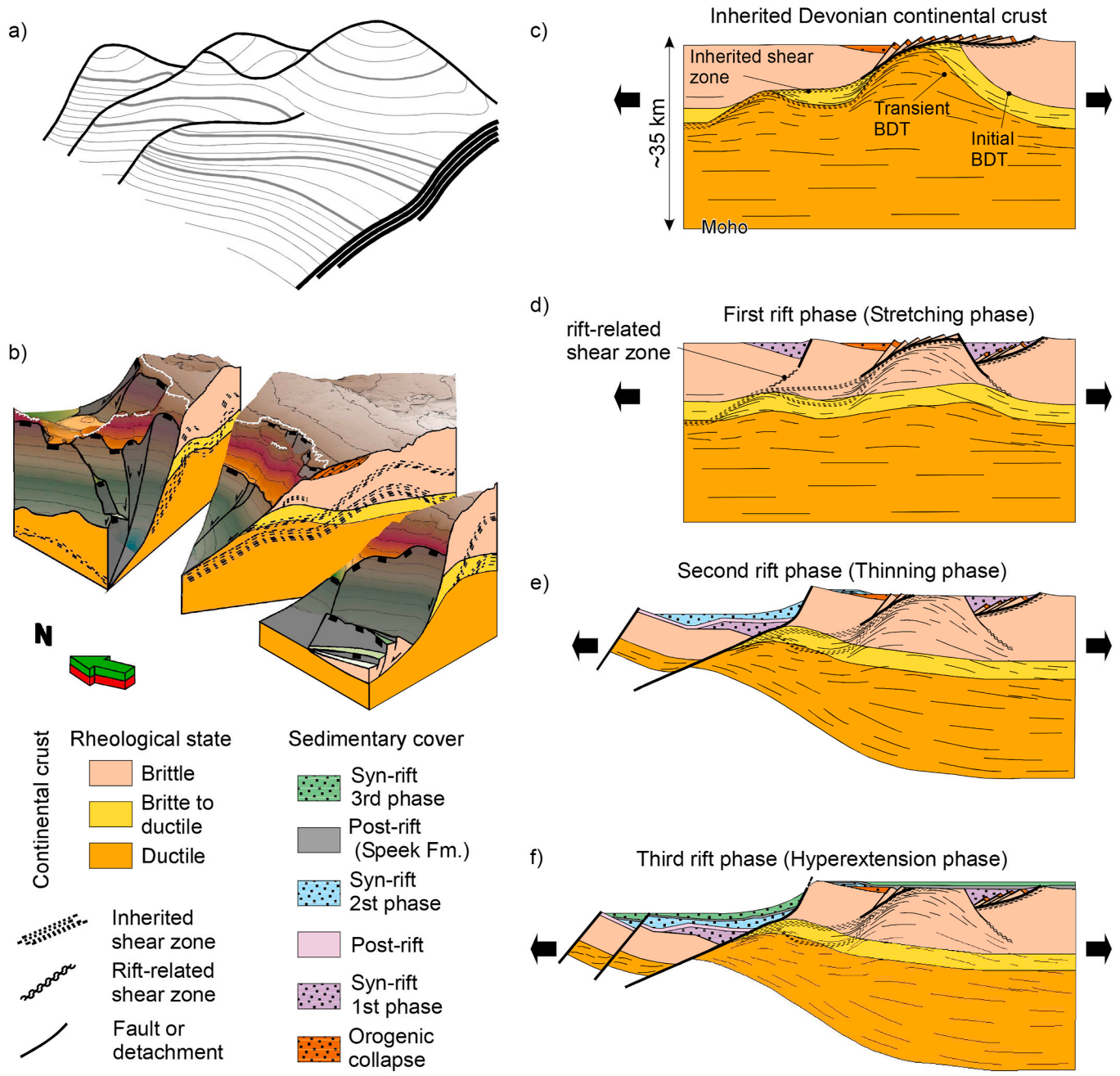

Fig. 16. Conceptual sketch of evolution of High-ß 'Type-1′ faults in a thick continental crust (>30 km). a) Hyperbolic geometry of the inherited shear zone mapped. b) Final 3D geometry of geometry of High-ß 'Type-1′ faults in a continental crust > thick. c) Inherited continental core complex. d) Development of half-grabens during first rift phase. e) Deformation localisation and formation of High-ß 'Type-1′ controlled for inherited shear zones during second rift phase. f) Final fault geometry after third deformation phase (Fig. 16c Adapted from Brun et al., 2018).

detachment.

8.2. *Role of structural inheritance at low-angle, high-displacement faults during the thinning deformation phase*

8.2.1. *The Klakk FC as a high-β 'Type 1' fault at the western flank of the Frøya High*

The Klakk FC has low-angle (*c.* 7°–23°), large-offset (*c.* 20–35 km) fault segments in our study area. This fault complex shows highly eroded footwalls, and the continental crust has a wedge shape in cross-section changing from *c.* 24 km to *c.* 11 km thick. Consequently, we confirm previous interpretations where the western Frøya High is the necking domain of the Norwegian Passive Margin (Faleide et al., 2008; Peron-Pinvidic et al., 2013; Mjelde et al., 2016; Osmundsen and Péron-Pinvidic, 2018). Following the Osmundsen and Péron-Pinvidic (2018) classification, these faults are High-β 'type-1'. We modified, however, the Peron-Pinvidic et al., 2013 and Osmundsen and Péron-Pinvidic, 2018 models for Klakk FC at the west of the Frøya High, showing the presence of combine and separated areas of inner and outer necking breakaways. We observe a considerable fault geometry variability in cross-section along strike: (i) the segments of the Klakk FC shows an upper part with >40° shallowing to *c.* 20° with depth on the northern structural salient; (ii) a small ridge divides the central recess into inner and outer necking breakaway zones; (iii) a single planar fault with *c.* 10° dips is located at the central structural salient; and (iv) segments of Klakk FC with an upper part > 40° that shallows to < 10° in

the southern structural recess. Our observations show that the Klakk FC has an inner- and outer-necking breakaway on the structural recesses, whereas the Klakk FC behaves as a combined inner and outer necking breakaway zone at the structural salients.

8.2.2. Role of the inheritance along the Klakk FC

The Frøya High is an offshore gneiss-core culmination, which is *c.* 120 km long with a general NNW-SSE strike. This High has been interpreted as a continental core complex and is the continuation of the CNBW (Skilbrei et al., 2002; Eide et al., 2005; Osmundsen et al., 2005; Maystrenko et al., 2018). Using the CNBW as an onshore analogue, we infer that the Frøya High must be composed by nappes, Devonian metamorphic core complexes and Devonian sedimentary basins. We interpret two continental core complexes to the west of the Frøya High, located within the northern and central structural salients respectively (Fig. 4). The locations of these core complexes coincide with the morphology of the hyperbolic geometry of SF4 at depth. This relationship leads us to postulate that the location and evolution of the continental core complexes controlled the geometry of the inherited shear zone, which subsequent controlled the location of the structural salients and recess during rifting. The geometry of the Devonian shear zones has been related to the exhumation and geometry of continental core complexes, as well as, with the geometry of the Devonian supradetachment basins onshore Norway (e.g. Figs. 2 and 3) (Osmundsen et al., 1998, 2006; Braathen et al., 2000; Vetti and Fossen, 2012; Wiest et al., 2019). Fig. 16c shows a likely geometry of the Frøya High area during late Devonian based on (i) the extrapolation of the SF4 shear zone geometry towards the top basement, (ii) the presence of granitic rock exhumed (376 ± 7 Ma) in the northern Frøya High (Eide et al., 2005), (iii) the continuation of the Høybakken detachment on the Frøya High (Osmundsen et al., 2002), (iv) the presence of high-grade metamorphic rocks with high magnetic values (>1200 nT) on the northern structural salient (Fig. 3b) (Skilbrei et al., 2002; Maystrenko et al., 2018), and (v) the presence of a Devonian basin on the Frøya High (Trice et al., 2019). This configuration may represent the inherited structural template for subsequent rifting phases.

Rheological variability related to inherited structures or lithology are candidates for what controlled the location of half-grabens on and around the Frøya High. Fault segments with high-dip angle in the upper part of the Klakk FC and the presence of faults that strike NE-SW suggest that some fault segments started as high angle faults during the stretching deformation phase (Permian-Lower Triassic). Widespread deformation that creates half-grabens within a continental crust of more-than 30 km thickness characterises the stretching deformation phase (Peron-Pinvidic et al., 2013; Naliboff et al., 2017). We, therefore, suggest that some faults with a NE-SW strike on the Klakk FC could have developed at the same time as the Mandel basin and some faults in the Froan Basin during the stretching deformation phase (Fig. 16d). This hypothesis cannot be reliably tested in the study area, however, because the footwall is highly eroded, the limits of resolution of seismic reflection data, and the lack of well data in the hanging wall.

The segments of the Klakk FC acquired its non-collinear structural configuration in map-view during the late Jurassic rifting phase (thinning deformation phase) (Fig. 16b and e). The thinning deformation phase is characterised by deformation migration and localisation, thinning of the middle-to-upper crust or lower crust-to-upper mantle, and generation of High-beta 'type 1′ faults that cause coupled deformation and the continental crustal wedge geometry (Peron-Pinvidic et al., 2013; Sutra et al., 2013; Manatschal et al., 2015; Naliboff et al., 2017). We observe these characteristics in the Klakk FC. In addition, this rift phase caused the denudation of the western part of the Frøya High, and generation of hyperextended half-grabens. The presence of a late Jurassic unconformity and a middle Cretaceous unconformity on the Frøya High (as identified in boreholes 6306/6-1, 6306/6-2) suggest that the faults reactivated during the early Cretaceous rifting phase (exhumation) (Figs. 4 and 16f). Continuation of footwall erosion and creation of west-directed canyons may have developed during this time.

The segments of the Klakk FC merged onto the SF4 shear zone when the Klakk FC became High-β 'type-1' during the thinning deformation phase (Fig. 16e). We observe that the lower part of the Klakk FC segments have a low-dip angle (>20°), and they tend to exhibit merging interaction (sensu Phillips et al., 2016) with the SF4 shear zone in the structural salients (Figs. 6–9). This interaction may become cross-cutting as it approaches the coupling fault. The role of the structural inheritance from pre-existing shear zones has been discussed in numerous studies using outcrop observations, seismic data and modelling (Osmundsen et al., 2002; Morley et al., 2004; Manatschal et al., 2015; Deng et al., 2017; Osagiede et al., 2020). These studies show that inherited shear zones may (i) accommodate major strain during the beginning of the thinning phase, (ii) deflect the stress orientation and influence the nearby younger faults, (iii) reactivate and propagate upwards as brittle faults, (iv) change the style of rift faulting, and (v) influence the final architecture of the necking zone. Based on these studies, we propose that deformation was localised on the Klakk FC area during the late Jurassic rifting phase. It reactivated the SF4 shear zone and caused faults to propagate upwards as brittle faults. These faults reached the surface or linked with faults generated during the first rifting phase (Fig. 16b and e).

Rift-related shear zones may be related to continental margin core complexes in the necking domain. The high displacement of the combined necking breakaway complex causes tectonic denudation and isostatic compensation, leading to exhumation of the middle crust. Osmundsen and Péron-Pinvidic (2018) interpret a continental margin core complex on the Gossa High based on the large-offset normal fault, the thinning of the continental crust, the geometry of the shear zone and the highly-rotated Upper Jurassic syn-rift deposits in the Slørebotn subbasin. A significant thickness of an inherited ductile shear zone or a hot type margin (sensu Clerc et al., 2018) is required to allow isostatic uplifting on the immediate footwall or crustal boudinage of the lower crust (Clerc et al., 2015, 2018; Osmundsen and Péron-Pinvidic, 2018). Although we did not observe highly-rotated Upper Jurassic sedimentary strata around the central structural salient of the Frøya High, we identified the other characteristics described on the Gossa High. It may suggest that the northwestern part of the central structural salient is a continental margin core complex that locally overprinted part of the SF4 shear zone.

Although the JML serves as a regionally important structural boundary between the Vøring and More margin segments (Blystad et al., 1995; Mjelde et al., 2016), and although the Klakk FC interacts interact to the south with the JML, we have found no evidence to suggest that the JML formed a key inheritance control on the structure and evolution of the Klakk FC proper (see e.g. Figs. 5e, 12b and 15 where the is no seismic evidence to suggest an underlying control of the JML). It cannot be ruled out, however, that the JML exercised some control on the fault control as it grew, partially affecting its southern termination; or a precursor structure of it, may have affected the evolution and geometry of the continental core complex at the time of its evolution, well before the Klakk FC develop.

8.3. Intra-basement shear zones in others high-displacement normal faults

High-displacement faults in necking domains with a thick continental crust have been recognised in the Iberian, Angolan, Santos, Campos, Socotra, Gulf of Lion, Newfoundland-Galicia rifted margins and the Great South Basin of New Zealand (Peron-Pinvidic et al., 2013; Sutra et al., 2013; Jolivet et al., 2010; Nonn et al., 2017; Phillips and McCaffrey, 2019). However, only Phillips and McCaffrey (2019) in the Great South Basin of New Zealand evaluate the role of inherited structures in the development of a high-displacement normal fault using two cross-sections. The geometries of the intra-basement reflections described in Phillips and McCaffrey (2019) are similar to the ones below the Klakk FC (this work), as well as, the ones interpreted by Koehl et al.

(2018) at the Barents Sea, though these are related to low-β faults.

Phillips and McCaffrey (2019) show that the High-β 'Terrane boundary fault' separates the Median Batholith (in its footwall) from the 'Western Province Terranes' (in its hanging wall). These authors associate the antiformal intra-basement reflections in the immediate fault's footwall with two structures. (i) a crustal shear zone with sub-parallel, dipping intra-basement reflections that are merging and thinning downwards along the 'Terrane boundary fault' in cross-section; (ii) a granitic laccolith with cross-cutting intra-basement reflections that form an antiform (See their Figs. 4 and 5). They interpret that the 'Terrane boundary' is an inherited shear zone or fault with two subsequent processes, an intrusion of a felsic body and fault reactivation because of change in the extension direction. Koehl et al. (2018) described the geometry of the Sørøy–Ingøya shear zone, which has similar antiformal intra-basement geometries in the immediate footwall of the Måsøy Fault Complex and Troms– Finnmark Fault Complex (see their Figs. 5 and 6). They interpret the high-amplitude intra-basement reflections packages as part of the Devonian Sørøy–Ingøya shear zone, which owe their geometry to the excision and incision process during the evolution of the Devonian shear zone. They also postulate that geometry of the Sørøy–Ingøya shear zone controlled the location and geometries of later rift-related structures. Our model presents another alternative for the interpretation of antiformal intra-basement reflections in the immediate footwall of high-β normal faults. As described early, we interpret that intra-basement reflections represent (i) an inherited Devonian (?) shear zone (SF4) and (ii) an Upper Jurassic (?) rift-related shear zone (SF3). Although we cannot discard intrusions completely, the seismic evidence suggests otherwise, and we favour Osmundsen and Péron-Pinvidic (2018) interpretation for the creation of Gossa High continental margin core complex. We suggest that the findings of findings of Phillips and McCaffrey (2019) support the ideas proposed herein, in indicating that inherited shear zones may control the final geometry of high-displacement (their Fig. 4), low-angle normal faults and, consequently, the geometry of the necking domains. This therefore validates the regional observations by Manatschal et al. (2015) for the architecture of necking domains in magma-poor rifted margins.

9. Conclusions

We have integrated potential field, well data, 2D and 3D seismic reflection data to address the role of structural inheritance during the development of high-displacement (>10 km), low-angle (>30°) normal faults in the necking domains of rifted margins with a thick continental crust (>25 km). We conclude that:

- The Klakk Fault Complex (Klakk FC) exhibits an overall N-S non-collinear pattern, which includes fault segments that locally strike NNW-SSE, NE-SW and N-S. These fault trends are strongly controlled by the location of two structural salients at the Frøya High.
- Klakk FC segments are generally high-β 'type 1' faults with listric or planar cross-sectional geometries. The Klakk FC has inner- and outer necking breakaway zones on the structural recesses, while it has combined inner and outer necking breakaway zones towards the west of the structural salients.
- The 3D structural mapping of intra-basement seismic facies allows us to recognise three structures, which are interpreted as a Devonian shear zone, a Devonian supradetachment basin, and a continental margin core complex (CMCC). We interpret the Devonian structures to be related to the orogenic collapse, while the CMCC to be a late Jurassic –early Cretaceous rift-related structure.
- SF4 shear zone may be a continuation to the west of the Devonian Høybakken Detachment. This shear zone has a hyperbolic geometry in three-dimension and their geometry has been locally modified by continental margin core complexes.
- The geometry of the continental core complex and inherited shear zone control the location of normal faults during the stretching deformation phase. Therefore, they generate the initial constraints in the development of structural salients and recesses.
- The mapped pre-existing shear zones place constraints on the final geometries of the high-β 'type 1' faults during the thinning deformation phase. Consequently, pre-existing intra-basement shear zones placed a large control on the geometry and evolution of the necking domain developed in a thick continental crust (>25 km).
- The interpreted structures and their control on the development of necking domains might be analogous to another areas with High-β 'type-1' faults in a thick continental crust (>25 km), such as the Iberian, Angolan, Santos, and Campos margins (Peron-Pinvidic et al., 2013), the Socotra margin (Noon et al., 2017), the Gulf of Lion (Jolivet et al., 2015) and the Newfoundland-Galicia margin (Sutra et al., 2013).

CRediT authorship contribution statement

Jhon M. Muñoz-Barrera: Conceptualization, Methodology, Formal analysis, Investigation, Writing - original draft, Writing - review & editing, Visualization. **Atle Rotevatn:** Conceptualization, Methodology, Validation, Formal analysis, Investigation, Resources, Writing - review & editing, Supervision, Funding acquisition. **Rob L. Gawthorpe:** Conceptualization, Methodology, Validation, Formal analysis, Investigation, Resources, Writing - review & editing, Supervision, Funding acquisition. **Gijs A. Henstra:** Conceptualization, Methodology, Validation, Formal analysis, Investigation, Writing - review & editing. **Thomas B. Kristensen:** Methodology, Validation, Formal analysis, Writing - review & editing.

Declaration of competing interest

The authors declare that they have no known competing financial interests or personal relationships that could have appeared to influence the work reported in this paper.

Acknowledgements

This contribution forms part of the Syn-Rift Systems Project funded by the Research Council of Norway, Aker BP, ConocoPhillips, DNO, Equinor, Neptune and Tullow Oil (project number 255229) to the University of Bergen and academic partners at the universities of Leeds, East Anglia, Lorraine and to the National and Kapodistrian University of Athens.

We thank Diskos, Tullow Oil and TGS for the 3D and 2D seismic data, Schlumberger for the Petrel interpretation software and Petroleum Experts for the Move structural software. We thank Yuriy Maystrenko for the Moho depth data, and Laurent Gernigon and Cecilie Hiorth for discussions about the Frøya High. We thank Vilde Dimmen, Christine Fichler, Jean-Baptiste Koehl, David Peacock, Johannes Wiest and Thilo Wrona for comments and suggestions. The lead author acknowledges the Norwegian Research School for Dynamics and Evolution of Earth and Planets (DEEP) and Research school on Changing Climates in the Coupled Earth System (CHESS) for the academic writing and illustration courses. Finally, we thank our reviewers, Gwenn Péron-Pinvidic and Thomas Phillips, whose insightful comments and suggestions led to significant improvements to this paper.

References

Andersen, A., Jamtveir, B., 1990. Uplift of deep crust during orogenic extensional collapse: a model based on field studies in the Sogn-Sunnfjord region of western Norway. Tectonics 9, 1097–1111. https://doi.org/10.1029/TC009i005p01097.

Andersen, T.B., Corfu, F., Labrousse, L., Osmundsen, P.T., 2012. Evidence for hyperextension along the pre-Caledonian margin of Baltica. J. Geol. Soc. 169, 601–612. https://doi.org/10.1144/0016-76492012-011.

Axen, G.J., 2004. Mechanics of low-angle normal faults. In: Karner, G.D., Taylor, B., Driscoll, N.W., Kohlstedt, D.J. (Eds.), Rheology and Deformation of the Lithosphere at Continental Margins. Columbia University Press, New York, USA.

Bell, R., Jackson, C., Elliott, G., Gawthorpe, R., Sharp, I.R., Michelsen, L., 2014. Insights into the development of major rift-related unconformities from geologically constrained subsidence modelling: Halten Terrace, offshore mid Norway. Basin Res. 26, 203–224. https://doi.org/10.1111/bre.12049.

Bird, P.C., Cartwright, J.A., Davies, T.L., 2015. Basement reactivation in the development of rift basins: an example of reactivated Caledonide structures in the West Orkney Basin. J. Geol. Soc. 172, 77–85. https://doi.org/10.1144/jgs2013-098.

Blystad, P., Brekke, H., Faerseth, R.B., 1995. Structural Elements of the Norwegian Continental Shelf. Pt. 2. The Norwegian Sea Region. Norwegian Petroleum Directorate.

Braathen, A., Nordgulen, Ø., Osmundsen, P.T., Andersen, T.B., Solli, A., Roberts, D., 2000. Devonian, orogen-parallel, opposed extension in the Central Norwegian Caledonides. Geology 28, 615–618. https://doi.org/10.1130/0091-7613(2000)28<615:DOOEIT>2.0CO;2.

Braathen, A., Osmundsen, P.T., Nordgulen, Ø., Roberts, D., Meyer, G.B., 2002. Orogen-parallel extension of the Caledonides in northern Central Norway: an overview. Norw. J. Geol. 82, 225–241.

Brun, J.-P., Sokoutis, D., Tirel, C., Gueydan, F., Van Den Driessche, J., Beslier, M.-O., 2018. Crustal versus mantle core complexes. Tectonophysics 746, 22–45. https://doi.org/10.1016/j.tecto.2017.09.017.

Chenin, P., Manatschal, G., Lavier, L.L., Erratt, D., 2015. Assessing the impact of orogenic inheritance on the architecture, timing and magmatic budget of the North Atlantic rift system: a mapping approach. J. Geol. Soc. 172, 711–720. https://doi.org/10.1144/jgs2014-139.

Clerc, C., Jolivet, J., Ringenbach, J.-C., 2015. Ductile extensional shear zones in the lower crust of a passive margin. Earth Planet Sci. Lett. 431, 1–7. https://doi.org/10.1016/j.epsl.2015.08.038.

Clerc, C., Ringenbach, J.-C., Jolivet, L., Ballard, J.-F., 2018. Rifted margins: ductile deformation, boudinage, continentward-dipping normal faults and the role of the weak lower crust. Gondwana Res. 53, 20–40. https://doi.org/10.1016/j.gr.2017.04.030.

Collagena, L., Jackson, C.A.-L., Bell, R.E., Coleman, A.J., Lenhart, A., Breda, A., 2019. Normal fault growth influenced by basement fabrics: the importance of preferential nucleation from pre-existing structures. Basin Res. 31, 659–687. https://doi.org/10.1111/bre.12327.

Corfu, F., Andersen, T.B., Gasser, D., 2014. The Scandinavian Caledonides: main features, conceptual advances and critical questions. Geol. Soc. 390, 9–43. https://doi.org/10.1144/SP390.25.

Daly, S.J., Chorowicz, J., Fairhead, J.D., 1989. Rift basin evolution in Africa: the influence of reactivated steep basement shear zones. In: Cooper, M.A., Williams, G.D. (Eds.), Inversion Tectonics. Geological Society, London, The UK, pp. 309–334. https://doi.org/10.1144/GSL.SP.1989.044.01.17.

Davis, G.A., Darby, B.J., Yadong, Z., Spell, T.L., 2002. Geometric and temporal evolution of an extensional detachment fault, Hohhot metamorphic core complex, Inner Mongolia, China. Geology 30, 1003–1006. https://doi.org/10.1130/0091-7613(2002)030<1003:GATEOA>2.0.CO;2.

Davis, G.H., 1980. Structural characteristics of metamorphic core complexes, southern Arizona. In: D Jr., C.M., Coney, P.J., Davis, G.H. (Eds.), Cordilleran Metamorphic Core Complexes. The Geological Society of America, Colorado, USA, pp. 35–77.

Deng, C., Gawthorpe, R.L., Finch, E., Fossen, H., 2017. Influence of a pre-existing basement weakness on normal fault growth during oblique extension: insights from discrete element modeling. J. Struct. Geol. 105, 44–61. https://doi.org/10.1016/j.jsg.2017.11.005.

Doré, A., Lundin, E., Jensen, L., Birkeland, Ø., Eliassen, P., Fichler, C., 1999. Principal tectonic events in the evolution of the northwest European Atlantic margin. In: Proceedings Geological Society, London, Petroleum Geology Conference Series, vol. 5. Geological Society of London, pp. 41–61.

Doré, A.G., Lundin, E., Fichler, C., Olesen, O., 1997. Patters of basement structure and reactivation along the NE Atlantic margin. J. Geol. Soc. 154, 85–92. https://doi.org/10.1144/gsjgs.154.1.0085.

Eide, E., Haabesland, N.E., Osmundsen, P.T., Andersen, T.B., Roberts, D., M A, K., 2005. Modern techniques and Old Red problems-determining the age of continental sedimentary deposits with 40Ar/39Ar provenance analysis in west-central Norway. Norw. J. Geol. 85, 133–149.

Elliott, G.M., Jackson, C.A.L., Gawthorpe, R.L., Wilson, P., Sharp, I.R., Michelsen, L., 2015. Late syn-rift evolution of the Vingleia Fault Complex, Halten Terrace, offshore Mid-Norway; a test of rift basin tectono-stratigraphic models. Basin Res. 1–23. https://doi.org/10.1111/bre.12158.

Elliott, G.M., Wilson, P., Jackson, C.A.L., Gawthorpe, R.L., Michelsen, L., Sharp, I.R., 2012. The linkage between fault throw and footwall scarp erosion patterns: an example from the Bremstein Fault Complex, offshore Mid-Norway. Basin Res. 24, 180–197. https://doi.org/10.1111/j.1365-2117.2011.00524.x.

Faleide, J.I., Bjørlykke, K., Gabrielsen, R.H., 2010. Geology of the Norwegian continental shelf. In: Landrø, M., Bjørlykke, K. (Eds.), Petroleum Geoscience: from Sedimentary Environments to Rock Physics. Springer, pp. 467–499. https://doi.org/10.1007/978-3-642-02332-3_22.

Faleide, J.I., Tsikalas, F., Breivik, A.J., Mjelde, R., Ritzmann, O., Engen, O., Wilson, J., Eldholm, O., 2008. Structure and evolution of the continental margin off Norway and the Barents Sea. Episodes 31, 82–91. https://doi.org/10.18814/epiiugs/2008/v31i1/012.

Fazlikhani, H., Fossen, H., Gawthorpe, R., Faleide, J.I., Bell, R.E., 2017. Basement structure and its influence on the structural configuration of the northern North Sea rift. Tectonics 36, 1151–1177. https://doi.org/10.1002/2017TC004514.

Fossen, H., 2000. Extensional tectonics in the caledonides: synorogenic or postorogenic? Tectonics 19, 213–224. https://doi.org/10.1029/1999TC900066.

Fossen, H., 2010. Extensional tectonics in the north Atlantic caledonides: a regional view. Geol. Soc. Spec. Publ. 335, 767–793. https://doi.org/10.1144/SP335.31.

Fossen, H., Cavalcante, G.C., 2017. Shear zones – a review. Earth Sci. Rev. 171, 434–455. https://doi.org/10.1016/j.earscirev.2017.05.002.

Fossen, H., Khani, H.F., Faleide, J.I., Ksienzyk, A.K., Dunlap, W.J., 2016. Post-Caledonian extension in the West Norway–northern North Sea region: the role of structural inheritance. Geol. Soc. Spec. Publ. 439 https://doi.org/10.1144/SP439.6. SP439.436.

Fossen, H., Rotevatn, A., 2016. Fault linkage and relay structures in extensional settings—a review. Earth Sci. Rev. 154, 14–28. https://doi.org/10.1016/j.earscirev.2015.11.014.

Friedmann, S.J., Burbank, D.W., 1995. Rift basins and supradetachment basins: intracontinental extensional end-members. Basin Res. 7, 109–127. https://doi.org/10.1111/j.1365-2117.1995.tb00099.x.

Gabrielsen, R.H., Odinsen, T., Grunnaleite, I., 1999. Structuring of the northern Viking Graben and the Møre basin; the influence of basement structural grain, and the particular role of the Møre-Trøndelag Fault Complex. Mar. Petrol. Geol. 16, 443–465. https://doi.org/10.1016/S0264-8172(99)00006-9.

Gawthorpe, R.L., Hall, M., Sharp, I., Dreyer, T., 2000. Tectonically enhanced forced regressions: examples from growth folds in extensional and compressional settings, the Miocene of the Suez rift and the Eocene of the Pyrenees. Geol. Soc. Spec. Publ. 172, 177–191. https://doi.org/10.1144/GSL.SP.2000.172.01.09.

Gee, M.J.R., Juhlin, C., Pascal, C., Robinson, P., 2010. Collisional orogeny in the scandinavian caledonides (COSC). GFF 132, 29–44. https://doi.org/10.1080/11035891003759188.

Gee, M.J.R., M, J., Majka, J., Robinson, P., van Roermuns, H., 2013. Subduction along and within the Baltoscandian margin during closing of the Iapetus Ocean and Baltica-Laurentia collision. Lithosphere 5, 169–178. https://doi.org/10.1130/L220.1.

Gernigon, L., Gaina, C., Olesen, O., Ball, P.J., Péron-Pinvidic, G., Yamasaki, T., 2012. The Norway Basin revisited: from continental breakup to spreading ridge extinction. Mar. Petrol. Geol. 35, 1–19. https://doi.org/10.1016/j.marpetgeo.2012.02.015.

Gernigon, L., Ringenbach, J.-C., Planke, S., Le Gall, B., Jonquet-Kolstø, H., 2003. Extension, crustal structure and magmatism at the outer Vøring Basin, Norwegian margin. J. Geol. Soc. 160, 197–209. https://doi.org/10.1144/0016-764902-055.

Gernigon, L., Franke, D., Geoffroy, L., Schiffer, C., Foulger, G.R., Stoker, M., 2020. Crustal fragmentation, magmatism, and the diachronous opening of the Norwegian-Greenland Sea. Earth Sci. Rev. 206, 102839. https://doi.org/10.1016/j.earscirev.2019.04.011, 1-37.

Henstra, G.A., Kristensen, T., Rotevatn, A., Gawthorpe, R., 2019. How do pre-existing normal faults influence rift geometry? A comparison of adjacent basins with contrasting underlying structure on the Lofoten Margin, Norway. Basin Res. 31, 1083–1097. https://doi.org/10.1111/bre.12358.

Jolivet, L., Gorini, C., Smit, J., Leroy, S., 2015. Continental breakup and the dynamics of rifting in back-arc basins: The Gulf of Lion margin. Tectonics 34, 663–679. https://doi.org/10.1001/2014TC003570.

Jolivet, L., Labrousse, L., Agard, P., Lacombe, O., Bailly, V., Lecomte, E., Mouthereau, F., Mehl, C., 2010. Rifting and shallow-dipping detachments, clues from the corinth rift and the Aegean. Tectonics 483, 287–304. https://doi.org/10.1016/j.tecto.2009.11.001.

Katumwehe, A.B., Abdelmalak, M.M., Atekwana, E.A., 2015. The role of pre-existing Precambrian structures in rift evolution: the Albertine and Rhino grabens, Uganda. Tectonophysics 646, 117–129. https://doi.org/10.1016/j.tecto.2015.01.022.

Kendrick, M.A., Eide, E., Roberts, A., Osmundsen, P.T., 2004. The Middle to Late Devonian Høybakken detachment, central Norway: ^{40}Ar-^{39}Ar evidence for prolonged late/post-Scandian extension and uplift. Geol. Mag. 141, 329–344. https://doi.org/10.1017/S0016756803008811.

Koehl, J.-B., Bergh, S.G., Henningsen, T., Faleide, J.I., 2018. Middle to late Devonian–carboniferous collapse basins on the Finnmark Platform and in the southwesternmost Nordkapp basin, SW Barents Sea. Solid Earth 9, 314–372. https://doi.org/10.5194/se-9-341-2018.

Lenhart, A., Jackson, C.A.-L., Bell, R.E., Duffy, O., Gawthorpe, R.L., Fossen, H., 2019. Structural architecture and composition of crystalline basement offshore west Norway. Lithosphere 11, 273–293. https://doi.org/10.1130/L668.1.

Lister, G.S., Etheridge, M.A., Symonds, P.A., 1986. Detachment faulting and the evolution of passive continental margins. Geology 14, 246–250. https://doi.org/10.1130/0091-7613(1986)14<246:DFATEO>2.0.CO;2.

Malavieille, J., 1993. Late orogenic extension in mountain belts: insights from the basin and range and the late Paleozoic Variscan belt. Tectonics 12, 1115–1130. https://doi.org/10.1029/93TC01129.

Manatschal, G., 2004. New models for the evolution of magma-poor rifted margins based on a review of data and concepts from West Iberia and the Alps. Int. J. Earth Sci. 93, 432–466. https://doi.org/10.1007/s00531-004-0394-7.

Manatschal, G., Lavier, L., Chenin, P., 2015. The role of inheritance in structuring hyperextended rift systems: some considerations based on observations and numerical modeling. Gondwana Res. 27, 140–164. https://doi.org/10.1016/j.gr.2014.08.006.

Marsden, D., 1989. I. Layer cake depth conversion. Lead. Edge 8, 10–14. https://doi.org/10.1190/1.1439561.

Masini, E., Manatschal, G., Mohn, G., Unternehr, P., 2012. Anatomy and tectono-sedimentary evolution of a rift-related detachment system: The example of the Err detachment (central Alps, SE Switzerland). GSA Bulletin 124, 1535–1551. https://doi.org/10.1130/B30557.1.

Maystrenko, Y., Gernigon, L., Nasuti, A., Olesen, O., 2018. Deep structure of the Mid-Norwegian continental margin (the Vøring and Møre basins) according to 3-D

density and magnetic modelling. Geophys. J. Int. 212, 1696–1721. https://doi.org/10.1093/gji/ggx491.
Mitchum, R.M., Vail, P.R., Sangree, J.B., 1977. Seismic stratigraphy and global changes of Sea level: Part 6. Stratigraphic interpretation of seismic reflection patterns in depositional sequences: section 2. Application of seismic reflection configuration to stratigraphic interpretation. In: Payton, C.E. (Ed.), Seismic Stratigraphy - Applications to Hydrocarbon Exploration. The American Association of Petroleum Geologists, Tulsa, USA, pp. 117–133. https://doi.org/10.1306/M26490C8.
Mjelde, R., Faleide, J.I., Breivik, A.J., Raum, T., 2009a. Lower crustal composition and crustal lineaments on the Vøring Margin, NE Atlantic: a review. Tectonophysics 472, 183–193. https://doi.org/10.1016/j.tecto.2008.04.018.
Mjelde, R., Goncharov, A., Müller, R., 2013. The Moho: Boundary above upper mantle peridotites or lower crustal eclogites? A global review and new interpretations for passive margins. Tectonophysics 609, 636–650. https://doi.org/10.1016/j.tecto.2012.03.001.
Mjelde, R., Kvarven, T., Faleide, J.I., Thybo, H., 2016. Lower crustal high-velocity bodies along North Atlantic passive margins, and their link to Caledonian suture zone eclogites and Early Cenozoic magmatism. Tectonophysics 670, 16–29. https://doi.org/10.1016/j.tecto.2015.11.021.
Mjelde, R., Raum, T., Kandilarov, A., Murai, Y., Takanami, T., 2009b. Crustal structure and evolution of the outer Møre Margin, NE Atlantic. Tectonophysics 468, 224–243. https://doi.org/10.1016/j.tecto.2008.06.003.
Mjelde, R., Raum, T., Shimamura, H., Murai, Y., Takanami, T., Faleide, J.I., 2005. Crustal structure of the Vøring Margin, NE Atlantic: a review of geological implications based on recent OBS data. In: Doré, A.G., Vining, B.A. (Eds.), Petroleum Geology: North-west Europe and Global Perspectives-Proceedings of the 6th Petroleum Geology Conference. The Geological Society, London, pp. 803–813. https://doi.org/10.1144/0060803.
Morley, C.K., Haranya, C., Phoosongsee, W., Pongwapee, S., Kornsawan, A., Wonganan, N., 2004. Activation of rift oblique and rift parallel pre-existing fabrics during extension and their effect on deformation style: examples from the rifts of Thailand. J. Struct. Geol. 26, 1803–1829. https://doi.org/10.1016/j.jsg.2004.02.014.
Mosar, J., 2003. Scandinavia's North Atlantic passive margin. J. Geophys. Res. 108, 1–18. https://doi.org/10.1029/2002JB002134.
Müller, R., Nystuen, J.P., Eide, F., Lie, H., 2005. Late Permian to Triassic basin infill history and palaeogeography of the Mid-Norwegian shelf - east Greenland region. In: Wandas, B. (Ed.), Onshore-offshore Relationships on the North Atlantic Margin. Norwegian Petroleum Society, pp. 165–189. https://doi.org/10.1016/S0928-8937(05)80048-7.
Naliboff, J.B., Buiter, S.J.H., Péron-Pinvidic, G., Osmundsen, P.T., Tetreault, J., 2017. Complex fault interaction controls continental rifting. Nat. Commun. 8, 1–9. https://doi.org/10.1038/s41467-017-00904-x.
Nasuti, A., Pascal, C., Ebbing, J., 2012. Onshore–offshore potential field analysis of the Møre–Trøndelag Fault Complex and adjacent structures of Mid Norway. Tectonophysics 518–521, 17–28. https://doi.org/10.1016/j.tecto.2011.11.003.
Noon, C., Leroy, S., Khanbari, K., Ahmed, A., 2017. Tectono-sedimentary evolution of the eastern Gulf of Aden conjugate passive margins: Narrowness and asymmetry in oblique rifting context. Tectonophysics 721, 322–348. https://doi.org/10.1016/j.tecto.2017.09.024.
Olesen, O., Ebbing, J., Gellein, J., Kihle, O., Myklebust, R., Sand, M., Skilbrei, J.R., Solheim, D., S, U., 2010. Gravity anomaly map, Norway and adjacent areas. Geol. Surv. Norway. Trondheim, Norway, Retreived from. https://www.ngu.no/en/publikasjon/gravity-anomaly-map-norway-and-adjacent-areas-scale-13-mill.
Olesen, O., Gellein, J., Gernigon, L., Kihle, O., Koziel, J., Lauritsen, T., Mogaard, J.O., Myklebust, R., Skilbrei, J.R., Usov, S., 2010b. Magnetic anomaly map, Norway and adjacent areas. Geol. Surv. Norway. Trondheim, Norway, Retrieved from. https://www.ngu.no/en/publikasjon/magnetic-anomaly-map-norway-and-adjacent-areas-scale-13-mill.
Osagiede, E., Rotevatn, A., Gawthorpe, R.L., Kristensen, T., Jackson, C.A.-L., Marsh, N., 2020. Pre-existing intra-basement shear zones influence growth and geometry of non-colinear normal faults, western Utsira High–Heimdal Terrace, North Sea. J. Struct. Geol. 130 https://doi.org/10.1016/j.jsg.2019.103908.
Osmundsen, P.T., Andersen, T.B., 2001. The middle Devonian basins of western Norway: sedimentary response to large transtensional tectonics? Tectonophysics 332, 51–68. https://doi.org/10.1016/S0040-1951(00)00249-3.
Osmundsen, P.T., Andersen, T.B., Markussen, S., Svendby, A.K., 1998. Tectonics and sedimentation in the hangingwall of a major extensional detachment: the Devonian Kvamshesten Basin, western Norway. Basin Res. 10, 213–234. https://doi.org/10.1046/j.1365-2117.1998.00064.x.
Osmundsen, P.T., Braathen, A., Sommaruga, A., Skilbrei, J.R., Nordgulen, Ø., Roberts, D., Andersen, T.B., Olesen, O., Mosar, J., 2005. Metamorphic core complexes and gneiss-cored culminations along the Mid-Norwegian margin: an overview and some current ideas. In: Wandås, B., Nystuen, J.P., Eide, E., Gradstein, F.M. (Eds.), Onshore-offshore Relationships on the North Atlantic Margin. Norwegian Geological Society, Norway, pp. 29–41. https://doi.org/10.1016/S0928-8937(05)80042-6.
Osmundsen, P.T., Ebbing, J., 2008. Styles of extension offshore mid-Norway and implications for mechanisms of crustal thinning at passive margins. Tectonics 27, 1–25. https://doi.org/10.1029/2007TC002242. TC6016.
Osmundsen, P.T., Eide, E., Haabesland, N.E., Roberts, D., Andersen, T.B., Kendrick, M.A., Bingen, B., Braathen, A., Redfield, T.F., 2006. Kinematics of the høybakken detachment zone and the Møre–Trøndelag Fault complex, central Norway. J. Geol. Soc. 163, 303–318. https://doi.org/10.1144/0016-764904-129.
Osmundsen, P.T., Péron-Pinvidic, G., 2018. Crustal scale fault interaction at rifted margins and the formation of domain-bounding breakaway complexes: insights from offshore Norway. Tectonics 37, 935–964. https://doi.org/10.1002/2017TC004792.
Osmundsen, P.T., Péron-Pinvidic, G., Ebbing, J., Erratt, D., Fjellanger, E., Bergslien, D., Syvertsen, S.E., 2016. Extension, hyperextension and mantle exhumation offshore Norway: a discussion based on 6 crustal transects. Norw. J. Geol. 96, 343–372. https://doi.org/10.17850/njg96-4-05.
Osmundsen, P.T., Redfield, T.F., 2011. Crustal taper and topography at passive continental margins. Terra. Nova 23, 349–361. https://doi.org/10.1111/j.1365-3121.2011.01014.x.
Osmundsen, P.T., Sommaruga, A., Skilbrei, J.R., Olesen, O., 2002. Deep structure of the Mid Norway rifted margin. Norw. J. Geol. 82, 202–2224.
Peron-Pinvidic, G., Manatschal, G., Osmundsen, P.T., 2013. Structural comparison of archetypal Atlantic rifted margins: a review of observations and concepts. Mar. Petrol. Geol. 43, 21–47. https://doi.org/10.1016/j.marpetgeo.2013.02.002.
Péron-Pinvidic, G., Osmundsen, P.T., Ebbing, J., 2016. Mismatch of geophysical dataset in distal rifted margin studies. Terra. Nova 28. https://doi.org/10.1111/ter.12226, 340-314.
Péron-Pinvidic, G., Osmundsen, P.T., 2018. The Mid Norwegian - NE Greenland conjugate margins: rifting evolution, margin segmentation, and breakup. Mar. Petrol. Geol. 98, 162–184. https://doi.org/10.1016/j.marpetgeo.2018.08.011.
Phillips, T., McCaffrey, K., 2019. Terrane boundary reactivation, barriers to lateral fault propagation and reactivated fabrics: rifting across the Median Batholith Zone, Great South Basin, New Zealand. Tectonics 38, 4027–4053. https://doi.org/10.1029/2019TC005772.
Phillips, T.B., Jackson, C., Bell, R., Duffy, O., Fossen, H., 2016. Reactivation of intrabasement structures during rifting: a case study from offshore southern Norway. J. Struct. Geol. 91, 54–73. https://doi.org/10.1016/j.jsg.2016.08.008.
Ravnås, R., Berge, K., Campbell, H., Harvey, C., Norton, M.J., 2014. Halten Terrace Lower and Middle Jurassic inter-rift megasequence analysis: megasequece structure, sedimentary architecture and controlling parameters. In: Martinius, A.W., Ravnås, R., Steel, R.J., Wonham, J.P. (Eds.), From Depositional Systems to Sedimentary Successions on the Norwegian Continental Margin. Wiley Blackwell, pp. 215–251.
Redfield, T.F., Braathen, A., Gabrielsen, R., Osmundsen, P.T., Torsvik, T.H., Andriessen, P.A.M., 2005. Late mesozoic to early cenozoic components of vertical separation across the Møre–Trøndelag Fault complex, Norway. Tectonophysics 395, 233–249. https://doi.org/10.1016/j.tecto.2004.09.012.
Reeve, M.T., Bell, R.E., Duffy, O., Jackson, C.A.-L., Sansom, E., 2015. The growth of non-colinear normal fault systems; what can we learn from 3D seismic reflection data? J. Struct. Geol. 70, 141–155. https://doi.org/10.1016/j.jsg.2014.11.007.
Reeve, M.T., Bell, R.E., Jackson, C.A.-L., 2014. Origin and significance of intra-basement seismic reflections offshore western Norway. J. Geol. Soc. 171, 1–4. https://doi.org/10.1144/jgs2013-020.
Ribes, C., Ghienne, J.-F., Manatschal, G., Decarlis, A., Karner, G.D., Figueredo, P.H., Johnson, C.A., 2019. Long-lived mega fault-scarps and related breccias at distal rifted margins: insights from present-day and fossil analogues. J. Geol. Soc. 176, 801–816. https://doi.org/10.1144/jgs2018-181.
Robinson, P., Gee, D., Roberts, D., Solli, A., Hollocher, K., Osmundsen, P.T., Grenne, T., van Roermund, H., Terry, M., Vrijmoed, H., Tucker, B., Krogh, T., Krill, A., Walsh, E., Regel, M., Daczko, N., 2015. A Tectonostratigraphic Transect across the Central Scandinavian Caledonides, Transcand Excursion. Geological Survey of Norway, Trondheim, Norway.
Rotevatn, A., Jackson, C.A.-L., 2014. 3D structure and evolution of folds during normal fault dip linkage. J. Geol. Soc. 171, 821–829. https://doi.org/10.1144/jgs2014-045.
Rotevatn, A., Kristensen, T., Ksienzyk, A.K., Wemmer, K., Henstra, G.A., Midtkandal, I., Grundvåg, S.-A., Andresen, A., 2018. Structural inheritance and rapid rift-length establishment in a multiphase rift: the East Greenland Rift System and its caledonian orogenic Ancestry. Tectonics 37, 1858–1875. https://doi.org/10.1029/2018TC005018.
Salazar-Mora, C.A., Huismans, R.S., Fossen, H., Egydio-Silva, M., 2018. The Wilson cycle and effects of tectonic structural inheritance on rifted passive margin formation. Tectonics 37, 3085–3101. https://doi.org/10.1029/2018TC004962.
Schiffer, C., Doré, A.G., Foulger, G.R., Franke, D., Geoffroy, L., Gernigon, L., Holdsworth, B., Kusznir, N., Lundin, E., McCaffrey, K., Peace, A., Petersen, K.D., Phillips, T., Stephenson, R., Stoker, M.S., Welford, K., 2019. Structural inheritance in the north Atlantic. Earth Sci. Rev. https://doi.org/10.1016/j.earscirev.2019.102975 (in press).
Seranne, M., 1992. Late Palaeozoic kinematics of the Møre-Trøndelag Fault zone and adjacent areas, central Norway. Nor. Geol. Tidsskr. 72, 141–158.
Serenne, M., Seguret, M., 1987. The Devonian basins of western Norway: tectonics and kinematics of an extending crust. In: Coward, M.P., Dewey, J.F., Hancock, P.L. (Eds.), Continental Extensional Tectonics. Geological Society, London, The UK, pp. 537–548. https://doi.org/10.1144/GSL.SP.1987.028.01.35.
Shaw, J.H., Connors, C., Suppe, J., 2004. Seismic Interpretation of Contractional Fault-Related Folds: an AAPG Seismic Atlas. The American Association of Petroleum Geologist, Tulsa, USA, p. 156.
Skilbrei, J.R., Olesen, O., 2005. Deep structure of the mid-Norwegian shelf and onshore-offshore correlations: insight from potential field data. In: Wandås, B., Nystuen, J.P., Eide, E., Gradstein, F.M. (Eds.), Onshore-Offshore Relationships on the North Atlantic Margin. NPF Special publication, Norway, pp. 43–68.
Skilbrei, J.R., Olesen, O., Osmundsen, P.T., Kihle, O., Aaro, S., Fjellanger, E., 2002. A study of basement structures and onshore-offshore correlations in Central Norway. Nor. Geol. Tidsskr. 82, 263–280.
Slagstad, T., Davidsen, B., Daly, S.J., 2011. Age and composition of crystalline basement rocks on the Norwegian continental margin: offshore extension and continuity of the Caledonian–Appalachian orogenic belt. J. Geol. Soc. 168, 1167–1185. https://doi.org/10.1144/0016-76492010-136.

Sutra, E., Manatschal, G., 2012. How does the continental crust thin in a hyperextended rifted margin? Insights from the Iberia margin. Geology 40, 139–142. https://doi.org/10.1130/G32786.1.

Sutra, E., Manatschal, G., Mohn, G., Unternehr, P., 2013. Quantification and restoration of extensional deformation along the Western Iberia and Newfoundland rifted margins. Geochem. Geophys. Geosyst. 14, 2575–2597. https://doi.org/10.1002/ggge.20135.

Tearpock, D., Bischke, R.D., 2003. Applied Subsurface Geological Mapping with Structural Methods, second ed. Prentice Hall PTR, New Jersey, p. 822.

Theuniseen, K., Klerkx, J., Melnikov, A., Mruma, A., 1996. Mechanisms of inheritance of rift faulting in the western branch of the East African Rift, Tanzania. Tectonics 15, 776–790. https://doi.org/10.1029/95TC03685.

Torsvik, T.H., Cocks, R.M., 2005. Norway in space and time: a Centennial cavalcade. Norw. J. Geol. 85, 73–86.

Trice, R., Hiorth, C., Holdsworth, R., 2019. Fractured basement play development on the UK and Norwegian rifted margins. In: Chiarella, D., Archer, S.G., Howell, J.A., Jackson, C.A.-L., Kombrink, H., Patruno, S. (Eds.), Cross-Border Themes in Petroleum Geology II: Atlantic Margin and Barents Sea. Geological Society, London. https://doi.org/10.1144/SP495-2018-174.

Tsikalas, F., Faleide, J.I., Eldholm, O., Blaich, O.A., 2012. The NE Atlantic conjugate margins. In: Roberts, D.G., Bally, A.W. (Eds.), Phanerozoic Passive Margins, Cratonic Basins and Global Tectonic Maps : Phanerozoic Passive Margins, Cratonic Basins and Global Tectonic Maps. Elsevier, Boston, USA.

Vetti, V., Fossen, H., 2012. Origin of contrasting Devonian supradetachment basin types in the Scandinavian Caledonides. Geology 40, 571–574. https://doi.org/10.1130/G32512.1.

Wernicke, B., 1981. Low-angle normal faults in the Basin and Range Province: nappe tectonics in an extending orogen. Nature 291, 645–648.

Whitney, D.L., Teyssier, C., Rey, P., Buck, W.R., 2013. Continental and oceanic core complexes. Geol. Soc. Am. Bull. 125, 273–298. https://doi.org/10.1130/b30754.1.

Wiest, J.D., Osmundsen, P.T., Jacobs, J., Fossen, H., 2019. Deep crustal flow within post-orogenic metamorphic core complexes – insights 1 from the southern Western Gneiss Region of Norway. Tectonics 38, 4267–4289. https://doi.org/10.1029/2019TC005708.

Wrona, T., Fossen, H., Lecomte, I., Eide, C.H., Gawthorpe, R.L., 2019. Seismic expression of shear zones: insights from 2-D convolution seismic modelling. EarthArXiv Pre-Print version. https://doi.org/10.31223/osf.io/5ypzg.